A derecho climatology (2004-2021) in the United States based on machine learning identification of bow echoes

Jianfeng Li[1, *], Andrew Geiss[1], Zhe Feng[1, *], L. Ruby Leung[1], Yun Qian[1], Wenjun Cui[2, 3]

[1]Atmospheric, Climate, and Earth Sciences Division, Pacific Northwest National Laboratory, Richland, Washington, USA

[2]Cooperative Institute for Severe and High-Impact Weather Research and Operations, University of Oklahoma, Norman, Oklahoma, USA

[3]National Severe Storms Laboratory, National Oceanic and Atmospheric Administration, Norman, Oklahoma, USA

*Correspondence to Jianfeng Li (jianfeng.li@pnnl.gov) and Zhe Feng (zhe.feng@pnnl.gov)

Abstract

Due to their persistent widespread severe winds, derechos pose significant threats to human safety and property, with impacts comparable to many tornadoes and hurricanes. Yet, automated detection of derechos remains challenging due to the absence of spatiotemporally continuous observations and the complex criteria employed to define the phenomenon. This study presents an objective derecho detection approach capable of automatically identify derechos in both observations and model results. The approach is grounded in a physically based definition of derechos and integrates three algorithms: (1) the Python Flexible Object Tracker (PyFLEXTRKR) algorithm to track mesoscale convective systems (MCSs), (2) a semantic segmentation convolutional neural network to identify bow echoes, and (3) a comprehensive classification algorithm to detect derechos within MCS lifecycles and distinguish derecho-producing from non-derecho-producing MCSs. Using this approach, we develop a novel high-resolution (4 km and hourly) observational dataset of derechos and accompanying derecho-producing MCSs over the United States east of the Rocky Mountains from 2004 to 2021. The dataset consists of two subsets based on different gust speed data sources and is analyzed to document the climatology of derechos in the United States. On average, 12-15 derechos are identified per year, aligning with previous estimations (~6-21 events annually). The spatial distribution and seasonal variation patterns are consistent with prior studies, showing peak occurrences in the Great Plains and Midwest during the warm season. Additionally, during the study period, derechos account for approximately 3.1% of measured damaging gusts (≥ 25.93 m s^{-1}) over the eastern United States. The dataset is publicly available at https://doi.org/10.5281/zenodo.14835362 (Li et al., 2025).

1 Introduction

A derecho is qualitatively defined as a widespread, long-lived straight-line windstorm associated with a fast-moving mesoscale convective system (MCS), and the latter is named a derecho-producing MCS (DMCS). Figure 1 shows two of the most destructive derechos and their accompanying DMCSs in the United States: the June 2012 North American derecho and the August 2020 Midwest Derecho. Both events lasted for over 10 hours, with apparent bow echoes and extensive damaging wind gusts (≥ 25.93 m s^{-1}). Due to the persistent widespread damaging gusts, derechos can severely damage property and threaten human lives, as exemplified by the extensive power outages and more than ten fatalities caused by the two derechos. Ashley and Mote (2005) demonstrated that derechos could be as hazardous as and were comparable in impact to most hurricanes and tornadoes in the United States between 1986 and 2003.

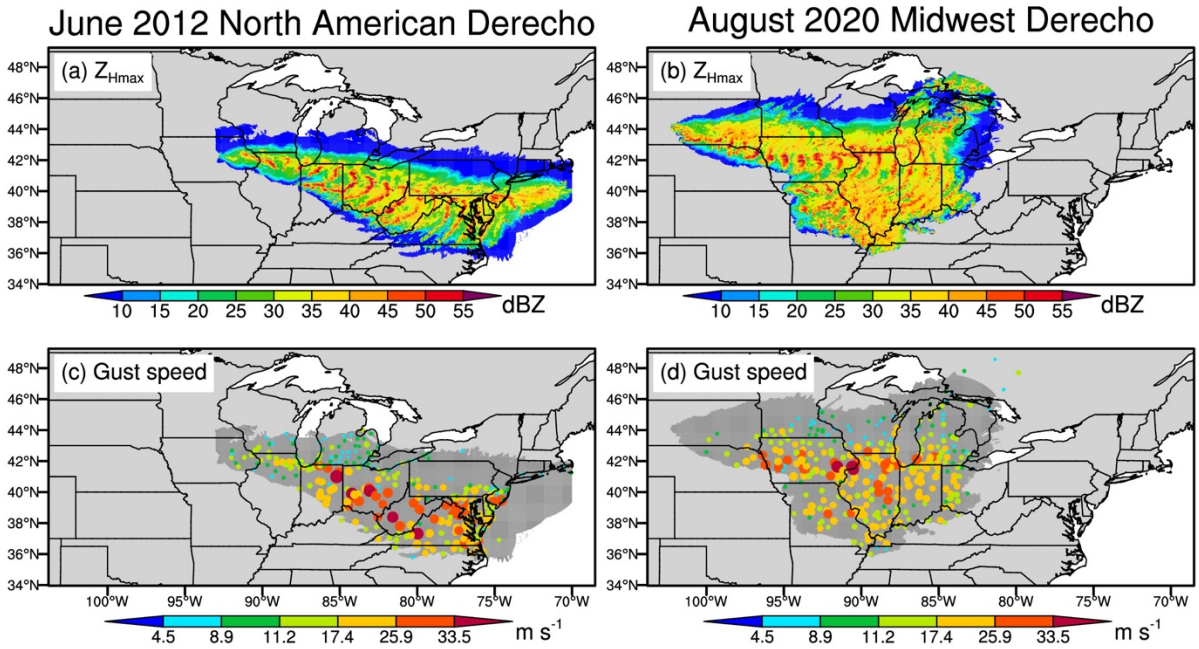

Figure 1. Spatial evolutions of the (a, b) composite (column-maximum) radar reflectivity (Z_{Hmax}) signatures and (c, d) surface gust speeds (colored dots) of two DMCSs. The first column is for the DMCS associated with the June 2012 North American derecho, which occurred on 29-30 June 2012, and the right column is the August 2020 Midwest derecho accompanying DMCS, which occurred on 10-11 August 2020. Due to spatiotemporal overlapping, multiple Z_{Hmax} and gust speeds may exist for a given grid cell or weather station, in which case only the corresponding maximums are shown in the figure. In (c) and (d), the dark gray shading refers to DMCS cold cloud coverage. The dot sizes in (c) and (d) are proportional to the gust speed magnitudes. Notably, gust speed in (c) and (d) is based on the hourly maximum gust speed ($gust_{hourly\_max}$), which is the largest gust speed within one hour if multiple gust speed measurements are available.

A reliable derecho dataset is foundational for understanding the underlying physical mechanism of derecho initiation and development and their socioeconomic impacts. Johns and Hirt (1987) developed the first derecho climatology in the warm seasons of 1980-1983 in the United States by quantitatively defining a derecho as a family of downburst clusters produced by an extratropical MCS. Specifically, they required a derecho to satisfy the following six criteria.

1) There must be a concentrated area of reports with wind damage or convective gusts > 25.7 m s^{-1}, and the major axis length of the area must be at least 400 km.
2) Those wind damage or convective gust reports must show a pattern of chronological progression, either as a singular swath or a series of swaths.
3) The concentrated area must have at least three reports of either F1 damage (32.7-50.3 m s^{-1}) (Fujita, 1971) or convective gust of at least 33.4 m s^{-1} separated by ≥ 64 km.
4) At most 3 hours can elapse between successive reports of wind damage or gust > 25.7 m s^{-1}.
5) The associated convective system must have temporal and spatial continuity in surface pressure and wind fields.
6) If multiple swaths of wind damage or gust reports > 25.7 m s^{-1} exist, they must be from the same MCS event.

Since then, several other studies have developed derecho climatologies during other periods using slightly different criteria (Bentley and Mote, 1998; Evans and Doswell, 2001; Bentley and Sparks, 2003; Coniglio and Stensrud, 2004; Guastini and Bosart, 2016). For example, Bentley and Mote (1998) removed the third requirement and reduced the elapsed time in the fourth condition from no more than 3 hours to no more than 2 hours in their derecho climatology from 1986 to 1996. In Coniglio and Stensrud (2004), the elapsed time was further changed to no more than 2.5 hours, and the gust reports of at least 33 m s^{-1} were used to separate derechos of different intensities.

Although the aforementioned derecho datasets were generated using different criteria and during different periods (Johns and Hirt, 1987; Bentley and Mote, 1998; Evans and Doswell, 2001; Bentley and Sparks, 2003; Coniglio and Stensrud, 2004; Guastini and Bosart, 2016), they showed many similar derecho climatological characteristics in the United States. For example, derechos occur more frequently in the warm than cold seasons; the Great Plains, Midwest, and Ohio Valley are regions most favorable for derecho development, and few derechos occur in the eastern and western coastal areas. Considering the inconsistent thresholds used in the above studies and the lack of physical mechanisms in their derecho definitions, Corfidi et al. (2016) proposed a stricter and more physically based derecho definition, which required the existence of sustained bow echoes with mesoscale vortices or rear-inflow jets and a nearly continuous wind damage swath of at least 100 km wide along most of its extent and 650 km long. In addition, the wind damage must occur after the convective system was organized into a cold-pool-driven forward-propagating MCS. Most derechos satisfying this definition would be classified as "progressive" but not "serial." A serial derecho typically originates in strongly forced environments and develops from a mature squall line with multiple embedded bow echoes. In contrast, progressive derechos generally originate from small convective clusters that grow upscale into large organized forward-propagating MCSs in synoptic environments with weak forcing (Squitieri et al., 2023).

It is difficult to develop a derecho climatology using the definition proposed by Corfidi et al. (2016) with current operational measurements, as it involves the identification of bow echoes, rear-inflow jets, and cold pools. However, rear-inflow jets and cold pools are generally associated with bow echoes (Weisman, 1993; Adams-Selin and Johnson, 2010). Once long-lived bow echoes are found in an MCS, we can expect the simultaneous existence of rear-inflow jets and cold pools. Nevertheless, identifying bow echoes, a feature typically identified visually from radar observations, is still challenging for large volumes of data, such as the 30+ year National Oceanic and Atmospheric Administration (NOAA) Next Generation Weather Radar (NEXRAD) archive consisting of 159 radars. The manual examination is time-consuming and sensitive to subjective biases. This study applies a semantic segmentation convolutional

neural network (CNN) to detect bow echoes automatically from two-dimensional composite (column-maximum) reflectivity (Z_{Hmax}) data in the United States, which are then combined with an MCS tracking dataset and surface gust speeds to identify derechos using criteria adjusted from Corfidi et al. (2016). After manual examination and validation, we produce a high-resolution (4 km and hourly) observational derecho and DMCS dataset in the United States east of the Rocky Mountains from 2004 to 2021. The dataset comprises two subsets based on different gust speed data sources: one uses gust speed measurements from the global hourly Integrated Surface Database (ISD) (NOAA/NCEI, 2001), and the other exploits gust speed reports from the NOAA's Storm Events Database (SED). As the first derecho climatology that utilizes a machine learning technique following physically based criteria and covers the recent decades, the dataset provides a reference for future derecho studies and can be used to investigate the underlying mechanisms for derecho initiation and development, the climatological impacts of derechos on hazardous weather, and the damage of derechos to infrastructure and human property.

The remainder of the paper is organized as follows. Section 2 introduces the MCS and gust speed datasets used to generate the derecho dataset. Section 3 describes the machine learning (i.e., semantic segmentation CNN) methodology to detect bow echoes, including sampling, training, and evaluation. Section 4 explains our derecho identification criteria in detail. Section 5 evaluates our derecho dataset through cross-validation of the two subsets (ISD-based vs. SED-based) and compare them with previous derecho estimations and the observational data from the NOAA Storm Prediction Center (SPC) in 2004 and 2005. Section 6 analyzes the derecho climatological characteristics. Section 7 shows how to access our derecho dataset, and the study is summarized in Section 8.

2 Source datasets

2.1 MCS dataset

Since previous MCS datasets only cover the period from 2004 to 2017 (Li et al., 2021; Feng et al., 2019), we use an updated version of the Python FLEXible Object TRacKeR (PyFLEXTRKR) software (Feng et al., 2023), which exploits collocated radar signatures, satellite infrared brightness temperature, and precipitation to identify robust MCS events (Feng et al., 2019), to produce an updated 4-km and hourly MCS dataset in the United States east of the Rocky Mountains from 2004 to 2021 (Feng, 2024). Several hourly source datasets are used in the generation of the MCS dataset, including the National Centers for Environmental Prediction (NCEP)/the Climate Prediction Center (CPP) L3 4 km Global Merged IR V1 brightness temperature dataset (Janowiak et al., 2017), the three-dimensional Gridded NEXRAD Radar (GridRad) dataset (Bowman and Homeyer, 2017), the NCEP Stage IV precipitation dataset (CDIACS/EOL/NCAR/UCAR and CPC/NCEP/NWS/NOAA, 2000), and melting level heights derived from ERA5 (European Centre for Medium-Range Weather Forecasts (ECMWF) Reanalysis v5) (Hersbach et al., 2023). The MCS definition criteria are almost the same as those in Feng et al. (2019), such as cold cloud shield (CCS) area > 60,000 km^2, precipitation feature (PF, which is a continuous convective or stratiform area with surface rain rate > 2 mm h^{-1}) major axis length > 100 km, the existence of 45-dBZ convective echoes, etc., except that the duration requirement is lowered to include those convective systems lasting for just 6 hours. This adjustment allows us to capture slightly shorter-lived MCSs that may produce intense wind gusts but are missed in the previous MCS datasets. Convective and stratiform radar echo classification in PyFLEXTRKR follows the Storm Labeling in 3D (SL3D) algorithm (Starzec et al., 2017), which uses horizontal texture and vertical structure of radar reflectivity from the GridRad product. Notably, the GridRad data are available each month from 2004 to 2017 but only between April and August from 2018 to 2021. Since most derechos occur in the warm season (Ashley and Mote, 2005; Coniglio and Stensrud, 2004), missing the cold months between 2018 and 2021

does not affect our derecho climatological analyses in Section 6. For brevity, we do not mention the missing cold months between 2018 and 2021 in the following sections unless stated otherwise.

2.2 Surface gust speed datasets

2.2.1 ISD gust speed measurements

The ISD is developed by the NOAA National Centers for Environmental Information (NCEI) in collaboration with several other institutions. ISD compiles global hourly and synoptic surface observations from numerous sources (e.g., the Automated Surface Observing System and the Automated Weather Observing System) into a single common format and data model. Besides internal quality control procedures conducted by the source datasets, ISD applies additional quality control algorithms to process each observation through a series of validity checks, extreme value checks, and internal and external continuity checks (Smith et al., 2011). This study uses ISD gust speed measurements passing all quality control checks (NOAA/NCEI, 2018). Notably, there may be multiple measurements at different times within one hour for some stations. To keep the sampling consistency across different datasets used in the derecho identification, we calculate $gust_{hourly\_max}$, which is the largest gust speed of all available measurements within one hour, for each observational site, unless stated otherwise. A total of 4,260 observational sites provide gust speed measurements between 2004 and 2021 in the study domain, of which 3,954 are over land, and the rest are over the ocean or lakes (Figure S1). We have excluded one observational site (ISD station ID: 726130-14755) in the northeastern United States, which has an unrealistic number of damaging gust measurements (more than 1,000 hours), inconsistent with the surrounding sites. We note that although we only use measurements passing all the available quality control checks, spatial quality control is missing in the ISD (Smith et al., 2011). Figure S2a shows that some sites in the eastern United States have apparently more damaging gust occurrences than their surrounding sites, but the occurrence frequencies are less than those stations around the Rocky Mountains. We do not have enough evidence to exclude them from the study. The quality of the ISD gust

speed measurements will undoubtedly be a source of uncertainty for our derecho dataset. In addition, only 420 ISD sites have continuous gust measurements from 2004 to 2021, while the rest have gust measurements only during part of the study period. The availability of ISD observational sites is another source of uncertainty when identifying derechos.

2.2.2 SED gust speed reports

The SED is also maintained by the NOAA NCEI and serves as NOAA's official publication documenting storms and other significant weather phenomena that are intense enough to cause socioeconomic damage (NOAA/NCEI, 2025). The National Weather Service (NWS) compiles storm data from a wide range of sources beyond meteorological weather stations and submits them to NCEI. These sources include, but are not limited to, local and federal law enforcement agencies, government officials, Skywarn spotters, NWS damage surveys, the insurance industry, newspaper clipping services, media reports, private companies, and individuals. While the NWS strives to use the best available information, some data in the SED remain unverified due to time and resource constraints. Consequently, the dataset suffers from inaccuracies, inconsistencies, and gaps (Santos, 2016). For example, Ardon-Dryer et al. (2023) found that half of the "dust storms" recorded in the SED had visibilities larger than 1 km, indicating misclassification, while many actual dust storms with visibilities of ≤ 1 km were missing from the dataset. These issues were attributed in part to the diverse sources contributing to the SED and the lack of systematic verification and consistency checks. Considering these limitations, particularly the fact that many strong (≥ 17.43 m s^{-1}) and damaging gust reports in the SED are estimated rather than measured, the derecho and DMCS dataset developed from SED in this study is published as a supplement to the dataset derived from the ISD.

From the SED, we extract measured and estimated gusts, along with their corresponding locations and timestamps, for the period from 2004 to 2021. The raw SED files are available at https://www.ncei.noaa.gov/pub/data/swdi/stormevents/csvfiles/ (NOAA/NCEI, 2025). If a gust report is

recorded as a segment, containing both a start and end location with respective timestamps, we process it as two independent reports: one at the start location and time and another at the end location and time. Although the accuracy of the SED gust speeds is not guaranteed, the database provides significantly more strong and damaging gust reports than the ISD due to its inclusion of estimated gusts from various sources. Approximately 82% of SED gust reports from 2004 to 2021 are estimated, while only 18% are measured. However, it is important to note that not all measured strong or damaging gusts are captured in the SED. Given the distinct limitations of both the ISD and SED datasets, we apply different thresholds criteria for derecho detection depending on the dataset used. These criteria are described in detail in Section 4.

3 Machine learning identification of bow echoes

A bow echo is a bow-shaped pattern with high reflectivity values on a radar image, but its vague definition makes it hard to identify them extensively and efficiently using traditional methods. Instead, we train a semantic segmentation CNN to identify bow echoes automatically from two-dimensional Z_{Hmax} images by performing pixel-level labeling of the bow echo extent. Compared to the manual examination of radar images, machine learning can save a tremendous amount of time and eliminate subjective bias.

3.1 Bow Echo Samples

3.1.1 Initial manual sampling

Our initial bow echo samples are generated based on the named derechos on Wikipedia (https://en.wikipedia.org/wiki/List_of_derecho_events; last access: 19 March 2023), corresponding to 54 accompanying DMCSs in the MCS dataset. We manually label times with apparent bow echoes through visual inspection of hourly Z_{Hmax} associated with the tracked DMCSs. Each positive sample is a 384 × 384-pixel (~1536 km × 1536 km) Z_{Hmax} image centered at the corresponding DMCS with a bow echo

embedded (Figure 2). The number of bow echo samples varies among different DMCSs, and 566 positive samples are obtained in total. 5400 negative samples are also randomly selected from the radar reflectivity dataset.

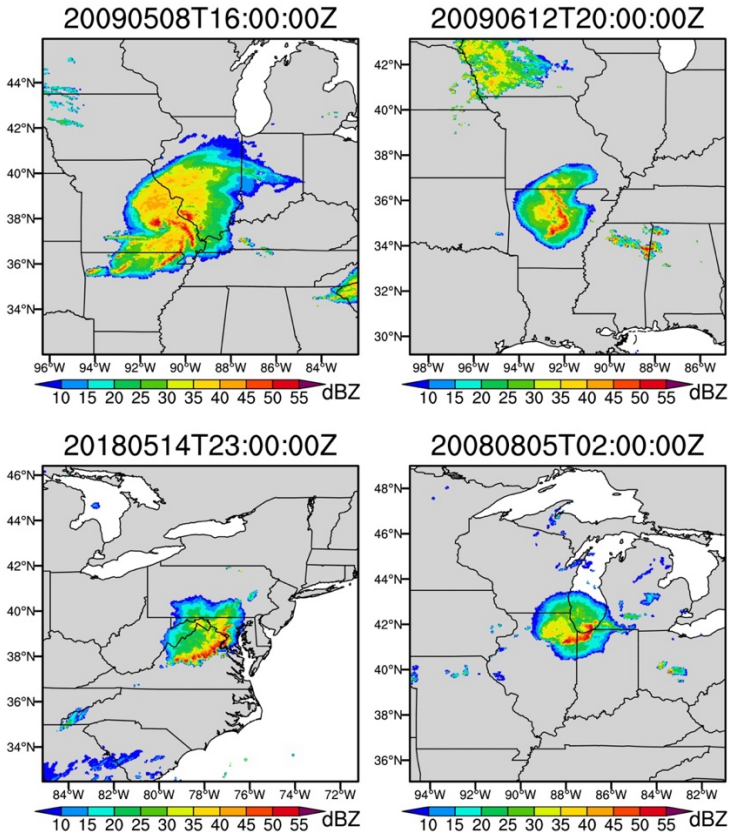

Figure 2. Four examples of bow echoes from the named derecho accompanying DMCSs. The color shading is for Z_{Hmax}. The subplot titles indicate the bow echo timings. For example, 20130613T04:00:00Z represents 4:00 UTC on 13 June 2013.

3.1.2 CNN-based selection of additional bow echo samples

Our initial attempt at developing an automated bow echo detection scheme is to train a classifier CNN — "Dense Net" (Huang et al., 2019) that ingests 384×384-pixel single-channel Z_{Hmax} images and outputs a single classification indicating the presence of a bow echo. Dense Nets are notable for their large number of skip connections (which create multiple paths for data to flow through the network without passing through every layer), and they can achieve comparable performance to very large classifier CNNs with only a fraction of the trainable parameters. Unfortunately, our manual inspection

finds that a Dense Net trained on the aforementioned initial samples has a very high false positive rate when applied to the full radar dataset. Although this Dense Net is unsuitable for deployment, the collection of new positive samples it successfully identifies allows us to supplement the list of known bow echoes and develop a more diverse training set for the following segmentation model.

3.1.3 Pseudo-labeling

By combining the initial samples and the manually selected true positives from the low-quality Dense Net model, we build a semantic segmentation training dataset of 500 unique bow echo snapshots and corresponding hand-drawn bow echo masks. While 500 positive samples are relatively small for a deep learning application, these samples have higher diversity than the initial bow echoes generated from the named derechos on Wikipedia because they are drawn from more distinct events, and, in general, semantic segmentation CNNs can be successfully trained with far fewer samples than image classification CNNs (Bardis et al., 2020).

A relatively low-skill version of the semantic segmentation CNN is trained using the 500 hand-labeled radar images and then applied to the entire Z_{Hmax} dataset. We manually review the bow echo masks produced by this segmentation model and add some of the high-quality masks to a new training dataset. We also collect some of its false positive masks as new negative samples in the new training dataset. This is a semi-supervised learning approach known as “pseudo-labeling” or “bootstrapping” (Van Engelen and Hoos, 2020; Ouali et al., 2020) and is commonly applied to semantic segmentation problems because of the high expense of hand-drawn labels (Peláez-Vegas et al., 2023). The pseudo-labels and hand-labels are combined into a final training dataset with 3677 samples, including 1699 bow echoes and 1978 negative samples, which is used to train the much more skillful semantic segmentation model in Section 3.2.

3.1.4 Data augmentation

To combat the limited training data further, we use several data augmentation strategies when constructing training batches. During training, positive and negative samples are selected with equal probability, and a batch size of 8 is used. First, random salt and pepper noise is added to 10% of the pixels in each sample with a probability of 0.1. Second, weak random Gaussian noise with a standard deviation of 5 dBZ is added to all the pixels in each sample with a probability of 0.1. Third, samples are flipped in up-down and left-right directions, each with a likelihood of 0.5. Fourth, samples are rotated by 0, 90, 180, or 270 degrees, each with a probability of 0.25. Fifth, samples are randomly shifted vertically and horizontally by -5 to 5 pixels. Sixth, the brightness of the sample image is adjusted by a random factor of -0.6 to +0.2, and the image contrast is randomly adjusted by -0.2 to 0.2. Seventh, the binary target bow echo masks are multiplied by 0.9, and random noise drawn from a uniform distribution between 0 and 0.1 is added. This is known as "soft labels." Lastly, both positive and negative samples are blended with randomly selected negative samples by taking the pixel-wise maximum reflectivity values of the two samples with a 0.5 likelihood. This last data augmentation is unusual but works well in our application because a) reflectivity features typically occupy only a fraction of the sample area, with most pixels being echo-free and b) bow echoes are high-reflectivity features. When the last data augmentation is applied to a positive sample, the resulting image will typically still contain a bow echo that matches the target mask well.

3.2 Training of U-Net 3+ CNN

Our final semantic segmentation CNN model (Figure 3) uses the U-Net 3+ architecture (Huang et al., 2020). U-Net 3+ is a modern variant of the U-Net architecture (Ronneberger et al., 2015) and differs from the U-Net primarily in the addition of many more skip connections and its multi-resolution loss, which computes loss on rescaled classification masks generated from feature representations at various model levels.

U-Net models were originally developed for the segmentation of biomedical imagery but have been applied to image segmentation problems in other fields and are broadly useful for any image-to-image mapping tasks where the input and target data are the same (or similar) size and shape and merging multi-resolution information from the input data is important. U-Net CNNs have been applied to a myriad of problems in the atmospheric sciences, such as segmentation (Galea et al., 2024; Kumler-Bonfanti et al., 2020), super resolution (Geiss and Hardin, 2020; White et al., 2024), physics parameterization (Lagerquist et al., 2021), downscaling (Sha et al., 2020), and weather forecasting (Weyn et al., 2021). Perhaps most closely related to this study is Mounier et al. (2022), who used a U-Net to detect bow echoes in simulated radar reflectivity images from a forecast model. A U-Net is an appropriate choice for the segmentation of bow echoes because merging multi-resolution information is crucial for identifying the feature. For example, bow echoes have high reflectivity at the pixel scale, strong reflectivity gradients in the transverse direction at the mid-scale (tens of pixels), and the characteristic bow shape at the large scale (hundreds of pixels).

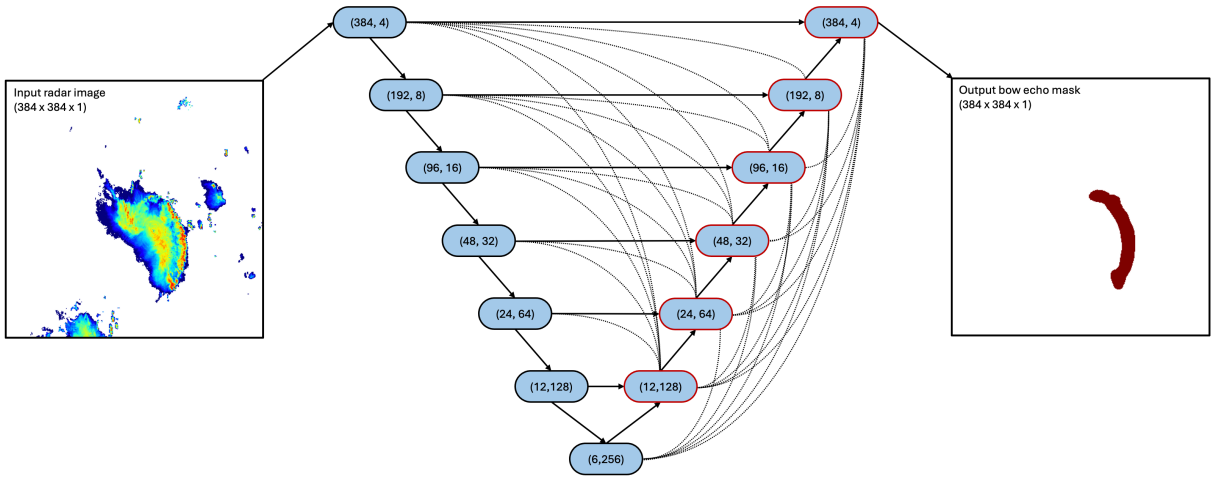

Figure 3. A diagram of our semantic segmentation CNN architecture. The CNN inputs a 384×384-pixel radar image (Z_{Hmax} scaled to 0-255) and outputs a bow echo mask of the same size. The blue ovals represent 3×3 convolutional layers, each followed by a batch normalization layer and a leaky rectified linear unit (ReLU) activation function. The first number in each blue oval indicates the spatial size (for both the width and height) of the output tensor, and the second represents the number of output channels. The solid arrows indicate connections in a standard U-Net architecture, with the downward arrows corresponding to 2×2 max-pooling and the upward arrows corresponding to 2×2 bilinear upsampling operations. The dashed lines represent the skip connections introduced in the U-Net 3+ architecture. These skip connections use max-pooling for spatial

downsampling and bilinear interpolation for upsampling, followed by a 16-channel 3×3 convolutional layer with a linear activation. Layers with multiple inputs use channel-wise concatenation to combine those inputs. During training, the output tensors from the layers in the upsampling branch (blue ovals with red boundaries) are scaled to the output spatial resolution and passed through a 1-channel 1×1 convolutional layer with sigmoid activation. Training loss is computed on all 6 of the resulting masks. At inference time, only the mask outputted from the upper-rightmost layer is used.

Our U-Net 3+ CNN ingests 384×384-pixel Z_{Hmax} images where Z_{Hmax} have been clipped to a 0-50 dBZ range and then linearly mapped to a range of 0-255. It is trained using binary cross entropy loss (Bishop, 2006) on masks generated from its 384, 192, 96, 48, 24, and 12-pixel resolution feature representations (Huang et al., 2020), though only the full-resolution (384×384-pixel) output mask is used at inference time. A detailed diagram of the model architecture is shown in Figure 3. Notably, although the model is trained using 384×384-pixel samples, it is a fully convolutional model and can process inputs of variable sizes.

We use the Adam optimizer (Kingma and Ba, 2014) with the Keras default settings (Ketkar, 2017) and an initial learning rate of 0.001 for training. The U-Net 3+ CNN is first trained for 60 epochs composed of 1000 randomly generated training batches of 8 samples each. Then, we decrease the learning rate to 0.0001 and train the CNN for an additional 20 epochs. The training duration is determined by performing an initial 5 rounds of training with 5-fold cross-validation and approximating the epoch numbers to reduce the learning rate and stop training when the mean intersection over union metric plateaus for the validation set. Instead of random shuffling, the validation sets are separated from the training dataset in temporally contiguous chunks to avoid any overlap because, sometimes, multiple samples may be drawn from different times of the same convective system.

3.3 Evaluation of the Semantic Segmentation CNN

We apply the trained U-Net 3+ CNN to the entire Z_{Hmax} dataset and obtain potential bow echo masks over the United States between 2004 and 2021 (Figure 4). As a final post-processing step, we ignore

323 "bow echo" masks with less than 20 pixels (~320 km^2), which are too small to be classified as bow
324 echoes.

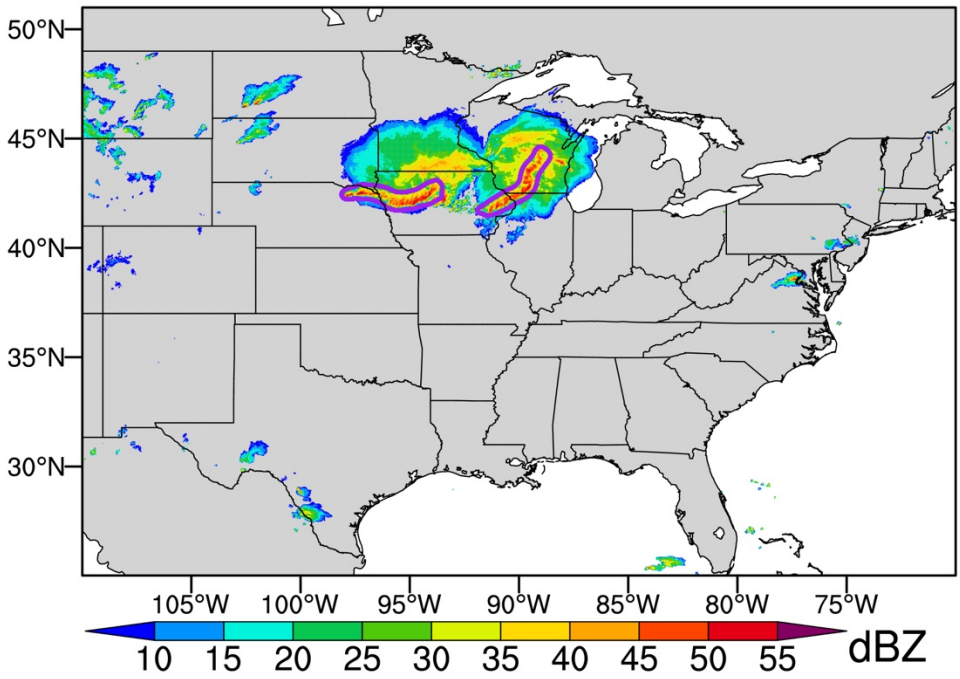

325
326 Figure 4. Examples of the U-Net 3+ CNN identified bow echoes (purple contours) based on Z_{Hmax} (color
327 shading) at 5:00 UTC on 17 June 2014.

328 Instead of validating our segmentation model at a pixel scale, as during the training stage, we prefer
329 evaluating its performance in detecting bulk bow echo features. In other words, we care about whether the
330 segmentation model can recognize the existence of bow echoes and capture their rough locations. Minor
331 spatial biases in bow echo coverage do not affect our below derecho identification much, which contains
332 various flexible criteria to minimize their impacts, such as the buffer zone within 100 km of bow echoes.
333 We also choose to validate the segmentation CNN specifically on MCS events where high reflectivity
334 features are present. Identifying low-reflectivity and echo-free images as non-bow echoes is desirable for
335 our segmentation model but trivial and not of particular interest for creating a derecho climatology.

336 To build a testing dataset, we randomly select 217 MCS-associated Z_{Hmax} images in 2010 based on
337 the following requirements. Each image is from a different MCS event. The images have variable sizes
338 and contain the full spatial extents of the MCSs at the selected times; however, they must be at least

192x192 pixels and cannot be drawn from a day that also has a sample in the training dataset. Three of the authors independently assessed the presence of bow echoes in each image, the results of which are then compared to the segmentation CNN (Table 1). Overall, the CNN model identifies 57 bow echoes, while human labelers 1, 2, and 3 identify 46, 76, and 66, respectively. The average human-human agreement and F_1 scores are 82% and 0.69, while the average human-CNN agreement and F_1 scores are 82% and 0.67 (Table 1). The test indicates that, on the one hand, the detection of bow echoes in radar images is prone to subjective bias; on the other hand, the performance of the segmentation CNN is comparable to that of a human in identifying bow echoes. We emphasize that the CNN bow echo identification is only one component in our following derecho detection criteria, and the adverse impact of this uncertainty is mitigated by other constraints (e.g., almost continuous bow echo existence and strong gusts in proximity with bow echoes).

Table 1 Evaluation of the performance of the segmentation CNN in the bow echo identification[1]

	CNN (57[2])	Person 1 (46)	Person 2 (76)	Person 3 (66)
CNN		84%	79%	83%
Person 1	0.66		77%	88%
Person 2	0.66	0.59		81%
Person 3	0.70	0.77	0.70	

[1]The upper triangular part of the table shows agreement between two independent identifications ($Agreement = \frac{TP+TN}{TP+TN+FP+FN}$), and the lower triangular part shows F_1 scores ($F_1 = \frac{2TP}{2TP+FP+FN}$), which is a better indication of the ability to agree on positives when positives are a minority (Taha and Hanbury, 2015). Here, *TP* denotes true positive, *TN* refers to true negative, *FP* is false positive, and *FN* is false negative. Notably, for the comparison between any two independent identifications, we consider one as "true" and evaluate the other against it (and which set of classifications is considered true does not impact these two metrics).

[2]The number of identified bow echoes from the 217 images.

We match the segmentation CNN detected bow echoes with MCS events from the MCS dataset and identify those MCS-associated bow echoes, which are used to identify derechos in the following section. Figure 5 shows the spatial distribution of MCS-associated bow echo occurrences from 2004 to 2021, which is similar to the MCS spatial distribution with more frequent occurrences in the Great Plains (Li et al., 2021).

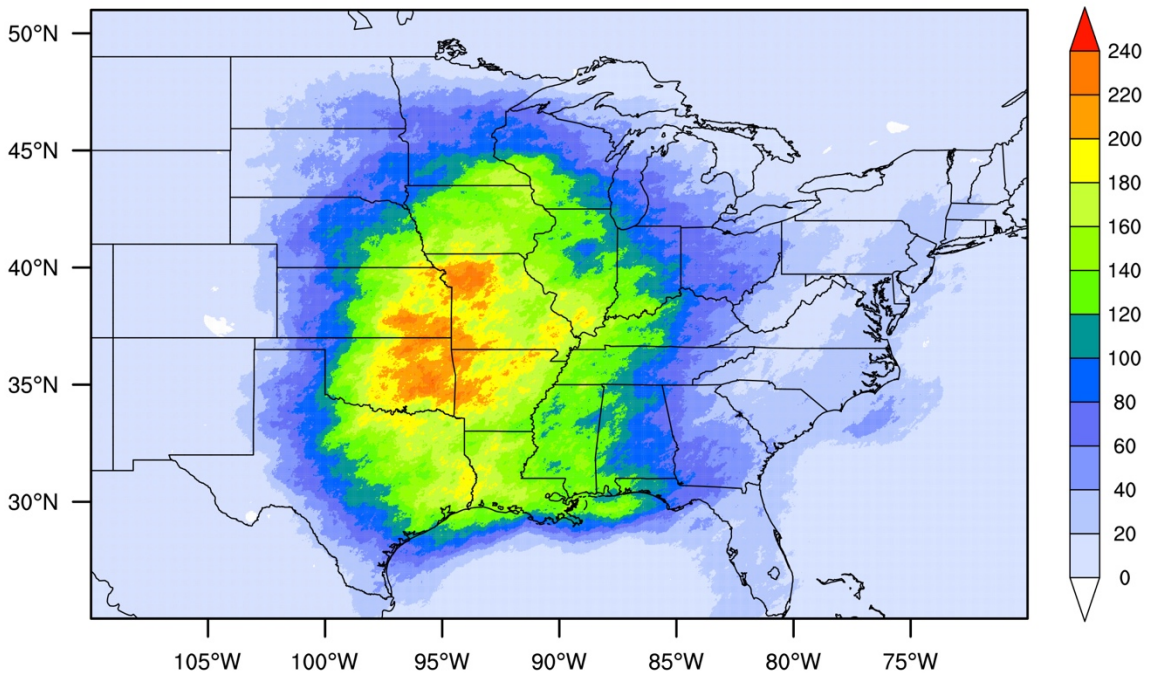

Figure 5. Spatial distribution of the number of MCS-associated bow echoes from 2004 to 2021. Here, we use bow echo masks produced by the segmentation CNN and exclude bow echoes that do not overlap with MCS events. This figure excludes bow echoes from those non-derecho-producing MCSs that overlap with tropical cyclones (TCs) from the International Best Track Archive for Climate Stewardship (IBTrACS) Version 4 data over the North Atlantic basin (Knapp et al., 2010) following the approach of Feng et al. (2021).

4 Derecho identification

4.1 Derecho definition

As mentioned above, we adopt the derecho definition proposed by Corfidi et al. (2016) but revise certain criteria based on previous studies (Johns and Hirt, 1987; Bentley and Mote, 1998) and dataset limitations to facilitate objective identification of derechos. Our final criteria are summarized below, with detailed explanations provided afterward (Figure 6).

1) A derecho must be attached to an MCS from the MCS dataset.
2) The derecho must persist for at least 5 hours, with a bow echo present for at least 80% of its lifetime. In addition, gaps between successive bow echo occurrences cannot exceed two hours.

All bow echoes must belong to the same bow echo series, as defined in the subsequent explanation.

3) The derecho bow echo series must exhibit forward propagation, based on two modified criteria from Corfidi et al. (2016):
    - The acute angle between the averaged bow echo orientation and the bow echo series' propagation direction must exceed 45° (Figure 6).
    - The propagation speed of the bow echo series must be at least 30% greater than the background mean wind speed at 500 hPa, derived from ERA5 data. The methodology for calculating the averaged bow echo orientation, bow echo series' propagation direction and speed, and the background mean wind speed is detailed in Appendix A.
4) Derecho-associated gust speed criteria vary based on the gust speed source dataset:
    - For ISD data: Within 100 km of the derecho-accompanied bow echoes (termed the "derecho area"), there must be at least 10 sites with strong gusts (≥ 17.43 m s^{-1}) and at least 1 site with damaging gusts (≥ 25.93 m s^{-1}).
    - For SED data: At least 10 locations must report damaging gusts.
    - The fraction of sites with strong/damaging gusts (ISD) or damaging gusts (SED) must be $\geq 20\%$.
    - Gaps between successive strong (ISD) or damaging (SED) gust reports cannot exceed two hours.
    - The gust swath must be at least 650 km in length and 100 km in width. Swath length and width calculations are explained below.

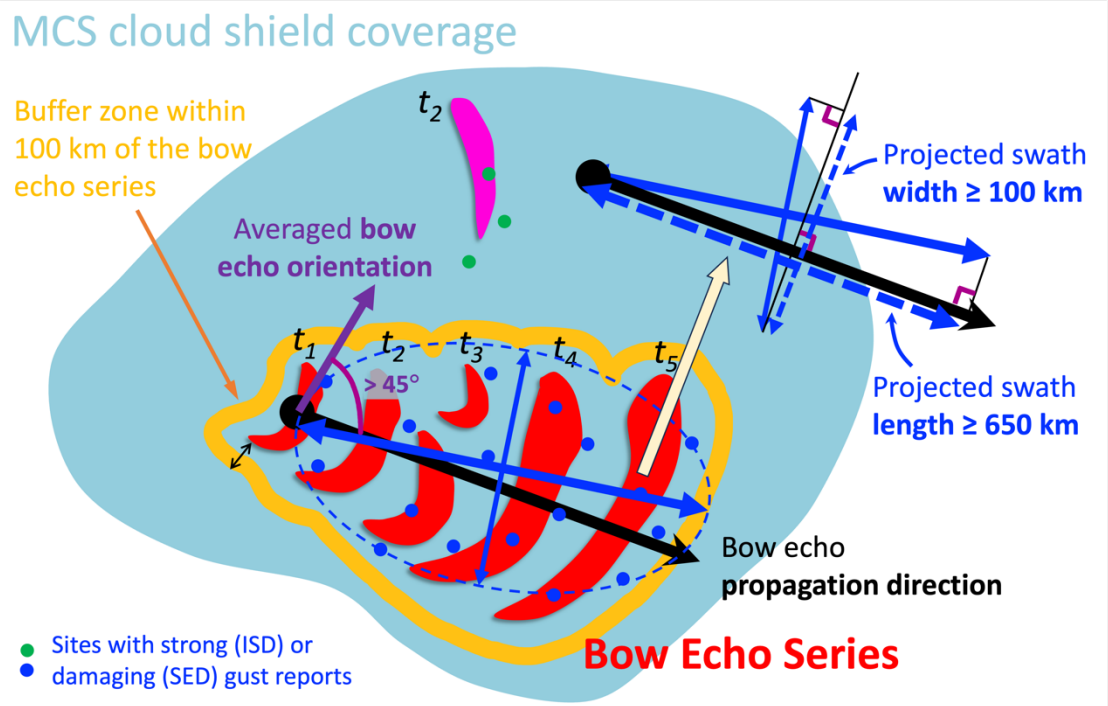

Figure 6. Schematic of the automated detection algorithm. Red and pink objects represent bow echoes. At time t_2, there are two bow echoes belonging to different bow echo series due to their great distance from each other. In contrast, the two bow echoes at t_3 are from the same bow echo series since they are close to each other. The pink bow echo at t_2 is far from the bow echoes at t_1 and t_3. Therefore, they belong to different bow echo series. The sites (green dots) with strong (for ISD) or damaging (for SED) gusts outside the 100-km buffer zone of the bow echo series (i.e., the derecho area) are excluded from the strong (ISD) or damaging (SED) gust swath calculation. The black arrow indicates the propagation direction of the bow echo series, and the violet arrow indicates the averaged bow echo orientation. Their acute angle must be > 45° for a derecho. The upper-right corner illustrates how the major and minor axis lengths of the gust fitted ellipse are projected onto another coordinate paralleling to the bow echo series' propagation direction to calculate gust swath length and width.

4.2 Explanation of Key Criteria and Adjustments

Criterion 1: MCS Association

This is a straightforward requirement and a major advantage of our approach. Due to the lack of a reliable MCS dataset, previous studies often spent considerable effort identifying spatiotemporally continuously propagating convective systems (Squitieri et al., 2023).

Criterion 2: Bow Echo Occurrence and Series Definition

418 The 80% bow echo occurrence threshold and the ≤ 2-hour lapse time between consecutive bow
419 echoes account for uncertainties in the segmentation CNN identification process and the diversity of MCS
420 events.

421 A bow echo series is defined in two steps:

422 1. Spatial grouping: Within a given MCS, bow echoes occurring in the same hour are categorized
423 into separate series if they are more than 100 km apart.
424 2. Temporal linking: Successive bow echoes (no more than 2 hours can elapse between their
425 occurrences) are considered part of the same series if they are less than 200 km apart, even if
426 they were initially classified as separate series.

427 Due to merging or splitting or the complex nature of some convective systems, a bow echo at one
428 hour may be far from the bow echoes right after or before that hour or another bow echo during that hour
429 (Figure 6). In such a rare situation, these bow echoes are unlikely caused by the same physical process
430 and, therefore, do not belong to the same bow echo series (Figure 6). The above stepwise approach
431 ensures that bow echoes from different physical processes are not incorrectly grouped.

432 Criterion 3: Forward Propagation Adjustment

433 We modify the Corfidi et al. (2016) criterion of "nearly orthogonal" to > 45° for the acute angle
434 between the averaged bow echo orientation and the bow echo series' propagation direction. This
435 adjustment:

436 • Accounts for segmentation CNN uncertainties, particularly in the propagation direction
437 estimation.
438 • Reduces false exclusions caused by minor variations in orientation.

439 Criterion 4: Gust Speed and Swath Calculation

The 20% fraction threshold is introduced to exclude MCSs potentially associated with extratropical cyclones, which often produce isolated strong or damaging gusts but weaker gusts across most sites.

To determine the gust swath length and width:

1. We fit an ellipse around sites with strong (ISD) or damaging (SED) gusts in the derecho area (Figure 6).
2. Since the ellipse may not align with the bow echo series' propagation direction, we project its major and minor axes onto a new coordinate system based on the bow echo propagation direction, as shown on the upper right corner of Figure 6. The projected major or minor axis length that is parallel to the bow echo propagation direction is the gust swath length, and the projected minor or major axis length that is perpendicular to the propagation direction is the swath width. Notably, both major and minor axis lengths can be projected parallelly and perpendicularly. If major axis length is projected parallelly, the minor axis length must be projected perpendicularly, and vice versa. Thus, we obtain two pairs of swath length and width.
3. We consider the uncertainties of the bow echo propagation direction when conducting the projection. In detail, we conduct projections iteratively by varying the propagation direction values with an interval of 0.2° within ±10° of the initial calculated bow echo series' propagation direction. Therefore, we obtain $\left(\frac{20}{0.2}+1\right)\times 2 = 202$ pairs of swath length and width in total. As long as one pair of swath length and width satisfies length ≥ 650 km and width ≥ 100 km, Criterion 4 is satisfied.

If no derecho is identified for a given MCS using the above definition criteria, we can relax the distance requirement (100 km) in Criterion 4 to be within 200 km of the derecho-associated bow echoes that satisfy the condition that there is no bow echo from the same bow echo series an hour ago or later during the derecho's lifetime. If the bow echo is in the first hour of the derecho's lifetime and there are no bow echoes for the corresponding MCS an hour ago, we can also extend the distance threshold to 200 km.

This is similar to the bow echo in the last hour of the derecho's lifecycle but without CNN-identified bow echoes an hour later. Notably, the distance extension is optional. For the bow echoes satisfying the above conditions, the distance threshold can be either 100 or 200 km. Using 100 km is superior to using 200 km until we find a derecho if it exists. The distance extension is also intended to minimize the impacts of the bow echo identification error. If a bow echo is missed in the semantic segmentation procedure, extending the distance threshold can include strong and damaging gusts associated with the missed bow echo, thus slightly reducing the derecho detection error.

We emphasize that, in Criterion 4, our ISD gust speed criteria are weaker than the SED gust speed criteria as well as those of previous studies (Squitieri et al., 2023; Bentley and Mote, 1998; Johns and Hirt, 1987), which also estimated the gust swath based on SED damaging gusts. As mentioned in Section 2.2.2, most SED gust reports are estimates, while ISD provides gust measurements from weather stations. SED estimates can capture potential damaging gust occurrences over a much larger area, although with large uncertainties. In contrast, due to the limited coverage of observational sites, real-time ISD measurements may miss substantial damaging gust occurrences in nearby regions. Therefore, we lower the gust speed criteria to capture potential derechos when using ISD measurements. It does not mean that the ISD-based derechos are weaker than the SED-based ones or even not derechos, as elaborated in Section 5.

4.3 Derecho detection results and postprocessing

Using ISD gust measurements, the objective detection algorithm identifies 245 derechos and associated DMCSs between 2004 and 2021. A notable example is the June 2012 North American derecho (Figure 7). Figure 7a displays the CNN-identified bow echoes of the DMCS, and Figure 7b shows the derecho area and associated gust speeds. As expected, the derecho produced widespread strong gusts.

To further refine the ISD dataset, we manually review all detected derechos and DMCSs, removing 31 false detections due to erroneous bow echo identification (Figure S3). In addition, we examine 1099 MCS events that produce extensive strong (≥ 10 observational sites) and damaging (≥ 1) gusts over land areas with a strong and damaging gust swath (fitted ellipse) of at least 650 × 100 km^2 (the ellipse's major and minor axis lengths). Our manual examination primarily focuses on bow echo identification errors but also slightly lower the forward propagating criteria thresholds for two potential derechos. For those MCSs that are potential DMCSs based on our visual inspection, we manually label their bow echo occurrences that fail the segmentation identification during potential derecho lifetimes (Figure S4) and rerun the automated derecho detection algorithm. Finally, 60 additional derechos are added, bringing the final total to 274 ($245 - 31 + 60 = 274$).

Using the same procedures for SED gust reports, we identify 220 derechos.

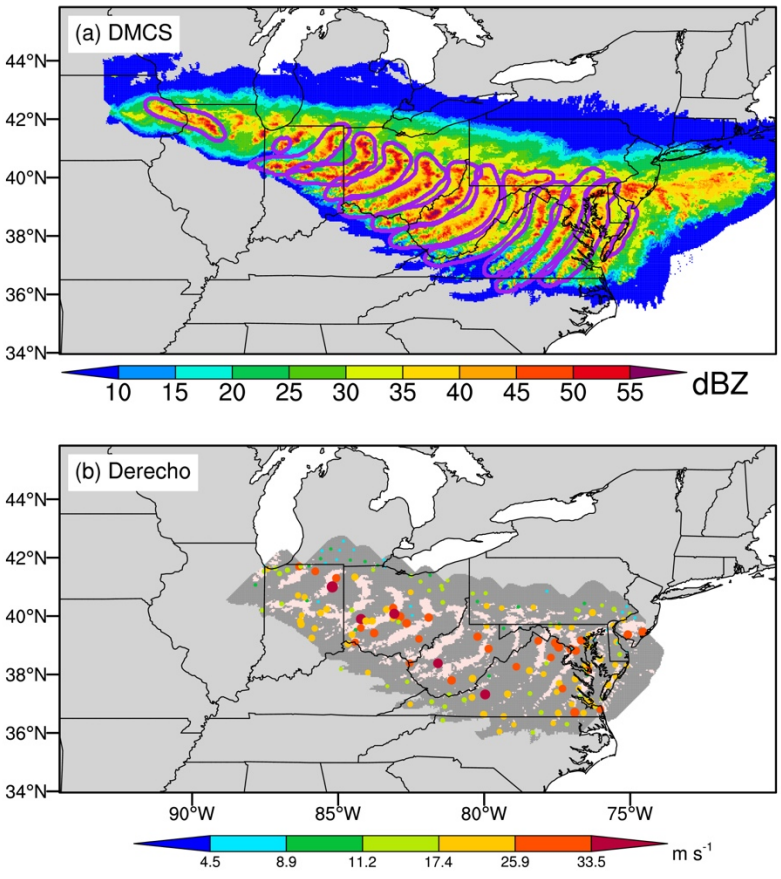

Figure 7. (a) Spatial evolution of Z_{Hmax} (color shading) and CNN-identified bow echoes (purple contours) from the DMCS associated with the June 2012 North American derecho. (b) Similar to (a) but for the derecho period. The derecho lasted from 17:00 UTC on 29 June to 6:00 UTC on 30 June 2012. The misty rose shading in (b) corresponds to $Z_{Hmax} \geq 40$ dBZ, while the gray shading refers to the derecho area. Colored dots are the same as those in Figure 1c, except only the derecho-associated gust measurements are shown.

5 Dataset evaluation and uncertainty

5.1 Evaluation against existing datasets

Between 2004 and 2021, our automated detection algorithm identifies 274 derechos (~ 15 per year) using ISD gust measurements and 220 derechos (~12 per year) using SED gust reports.. These numbers fall within the range of previous estimations (6.1-20.9 per year) based on a 400 km swath length threshold and conventional derecho definitions, as introduced in Section 1 (Squitieri et al., 2023; Johns and Hirt, 1987; Bentley and Mote, 1998; Evans and Doswell, 2001; Guastini and Bosart, 2016; Ashley and Mote, 2005). However, our derecho counts are substantially higher than those reported by Corfidi et al. (2016), who identified only 25 derechos in the warm seasons of 2010-2014 using a 650 km swath length threshold. These discrepancies likely stem from differences in the methods used to calculate gust swath length and width, the criteria for forward propagation, and the diverse observational source datasets used in the derecho detection.

To further evaluate our dataset, we compare it against the NOAA Storm Prediction Center (SPC) derecho data from 2004 and 2005 (https://www.spc.noaa.gov/misc/AbtDerechos/annualevents.htm; last access: November 17, 2023) (Table 2). This dataset provides detailed timings and locations of derechos or convective windstorms of near-derecho size, and it is the only available dataset that we can use to evaluate our derecho dataset at the event scale. However, it is important to note that the NOAA SPC data does not explicitly distinguish between derechos and convective windstorms of near-derecho size, and it relies on the conventional derecho definition, which can significantly influence derecho counts. Additionally, the NOAA SPC data is based on SED gust reports and lacks an underlying MCS database.

The NOAA SPC dataset contains 50 derechos and near-derecho size convective windstorms for 2004 and 2005, 15 of which are detected by our algorithm using ISD gust measurements. The number increases to 19 when using SED gust reports. Five of the 50 events are entirely absent in our MCS dataset, possibly because their associated MCSs moved too rapidly to satisfy PyFLEXTRKR's 50% areal overlap criterion using hourly satellite and NEXRAD dataset, or they failed to meet other MCS requirements in PyFLEXTRKR (Feng et al., 2019). The remaining discrepancies arise from factors such as an insufficient number of damaging gust reports or bow echoes, too small a gust swath, or lack of forward propagation. Conversely, our detection algorithm identifies several derechos (4 from ISD and 3 from SED) that are not present in the NOAA SPC dataset. Overall, while most derechos identified by our algorithm are captured in the NOAA SPC data, our derecho counts are notably lower due to our stricter physically-based derecho definition, which reduces the number of events classified as derechos compared to conventional definitions.

Cross validation between the ISD-based and SED-based datasets further supports the robustness of our detection algorithm (Figure 8). A total of 172 derechos are detected by both datasets, while 48 events are identified only in SED and 102 events are unique to ISD. Figure 8 also highlights discrepancies between the two datasets, with more ISD-based than SED-based derechos in 2008, 2010, 2014, 2015, 2019, and 2020, while their counts remain similar in other years. Despite these differences, the two datasets exhibit similar interannual variability, with a temporal correlation coefficient of 0.72. The general agreement between the two datasets support our decision to use different gust speed thresholds for ISD and SED in the detection algorithm. However, the observed discrepancies also underscores the critical role of the source datasets in influencing detection results, highlighting the need for more reliable gust speed observations.

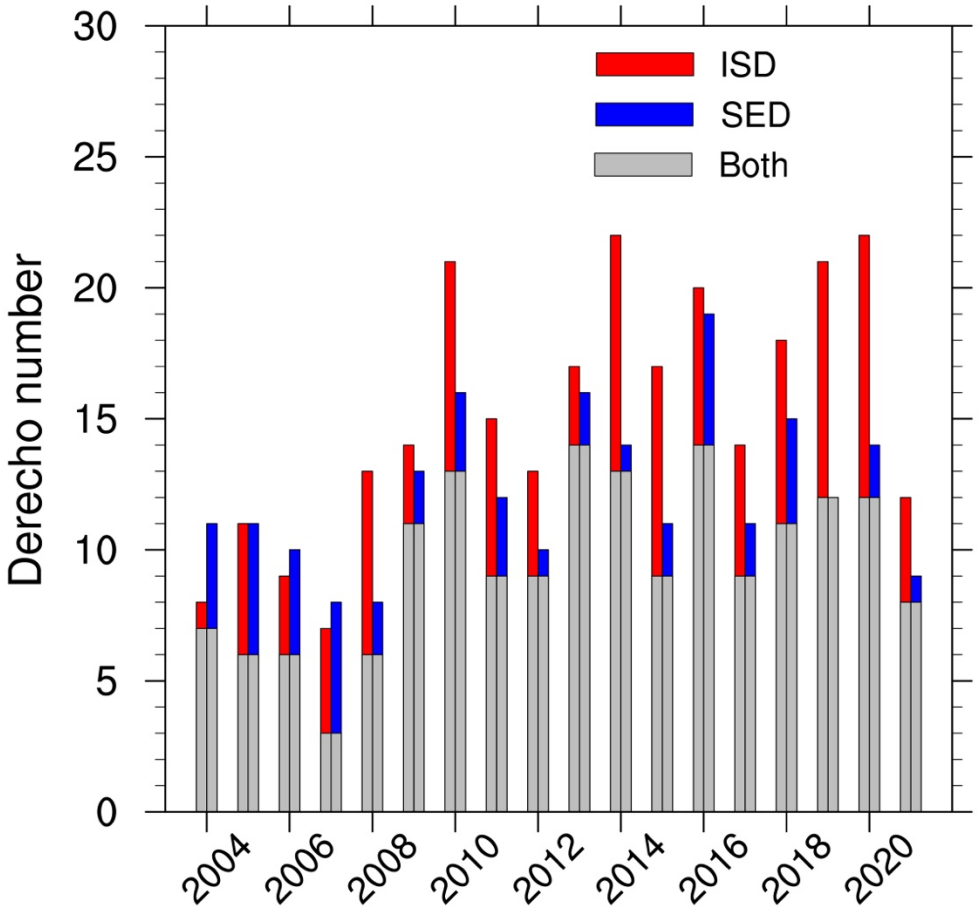

Figure 8. Bar chart of the annual derecho numbers from the ISD-based and the SED-based datasets from 2004 to 2021. Gray shading denotes derechos captured by both datasets, red shading refers to derechos only identified when using ISD gust observations, and blue shading represents SED-only derechos.

549 **Table 2. Evaluation of our derecho dataset against the NOAA SPC data in 2004 and 2005**

	Year 2004	Year 2005	Sum
NOAA SPC	24	26	50
Captured by the ISD dataset	7	8	15
Captured by the SED dataset	10	9	19
Derechos in ISD but not in NOAA SPC	1	3	4
Derechos in SED but not in NOAA SPC	1	2	3
NOAA SPC events missed in the MCS dataset	2	3	5

550

5.2 Discussion on dataset uncertainty

Besides the uncertainties in gust speed observations, we acknowledge additional sources of uncertainty affecting our dataset.

5.2.1 Uncertainty from the MCS dataset

As noted in our evaluation against the NOAA SPC data, uncertainties arise from the MCS dataset used in derecho detection. The 50% areal overlap threshold in PyFLEXTRKR, which links consecutive cold cloud shields (CCSs), may fail to capture very fast-moving convective systems using hourly satellite and NEXRAD data. Lowering this threshold would undoubtedly increase the number of identified MCSs and derechos, but it could also introduce false tracks that do not belong to the same storm system. The 50% threshold is widely used in various versions of the FLEXTRKR algorithms (Li et al., 2021; Feng et al., 2023; Feng et al., 2019) and other tracking algorithms based on overlap (e.g., (Whitehall et al., 2015)). While we maintain this threshold in our study, users should be aware of uncertainties related to adjustable parameters (e.g., areal overlap threshold, MCS duration, and major axis length) and limitations in the observational datasets used by PyFLEXTRKR (Feng et al., 2019; Li et al., 2021).

5.2.2 Uncertainty from the bow echo identification

Another key uncertainty arises from the segmentation CNN used to identify bow echoes. While our evaluation in Section 3.3 confirms high accuracy, we acknowledge that some derechos may be missed, while some non-derechos may be falsely classified as derechos due to the bow echo identification errors. To mitigate this issue, we conducted extensive manual verification of derecho and DMCS events, as well as other MCS events producing widespread strong gusts. However, the manual examination introduces subjective biases, and completely eliminating bow echo identification uncertainties remains challenging.

5.2.3 Uncertainty from derecho definition criteria

Our detection algorithm relies on several adjustable parameters and methodological choices, all of which influence the number of identified derechos. For example, if we require at least three very damaging gust reports (≥ 33.53 m s^{-1}) when using SED, the derecho count decreases from 220 to 149. As the first climatological derecho dataset to incorporate bow echoes and provide detailed event tracking, a full uncertainty assessment of all tunable parameters is beyond the scope of this study. However, our sensitivity tests indicate that changes to key parameters (e.g., reducing the strong gust fraction threshold to 10% or the number of sites with strong gust reports to 5) do not substantially alter the derecho spatial distribution or seasonal variation patterns (see Section 6). Furthermore, our dataset is designed to be flexible: we store all key parameters, allowing users to apply stricter thresholds if needed to focus on stronger derechos.

In summary, although our automated detection algorithm employs a physical-based derecho definition rather than conventional definitions, our derecho counts are comparable to or slightly lower than previous estimations, which is expected given our stricter criteria. Cross-validation between ISD-based and SED-based datasets supports the high quality of our derecho dataset and the reliability of our detection algorithm. However, users should be aware of the various sources of uncertainty in the dataset generation, particularly those related to gust speed observations, MCS tracking criteria, bow echo identification, and the choice of derecho definition parameters.

6 Derecho climatological characteristics

We primarily use the ISD-based derecho dataset to conduct the following climatological analyses, unless stated otherwise.

6.1 Annual statistics

Figure 8 displays the annual derecho numbers from 2004 to 2021. There is an apparent jump in the derecho number before (~10 derechos per year) and after 2007 (~15 derechos per year), which may be partially related to the general increase in the number of gust speed observational sites from 2004 to 2010 (Figure S5). Figure 9 shows the spatial distribution of yearly averaged annual ISD-based derecho numbers between 2004 and 2021. The central Great Plains has the most frequent derecho occurrences, extending to Oklahoma in the south, Iowa in the north, Kansas in the west, and Illinois in the east. The areas with frequent derecho occurrences are generally consistent with previous studies (Coniglio and Stensrud, 2004; Guastini and Bosart, 2016; Johns and Hirt, 1987; Ashley and Mote, 2005), although some differences are identified. For example, several studies identified a remarkable northwest-southeast axis with frequent derecho occurrences extending from southern Minnesota to Ohio, which is observable but not apparent in our spatial distribution (Johns and Hirt, 1987; Coniglio and Stensrud, 2004; Guastini and Bosart, 2016). The differences can be caused by many factors, such as distinct derecho definitions and observational datasets used in these studies. When we use SED gust reports in derecho detection, the spatial distribution of derecho counts shows a more noticeable northwest-southeast axis but with lower derecho numbers than the ISD-based dataset (Figure S6).

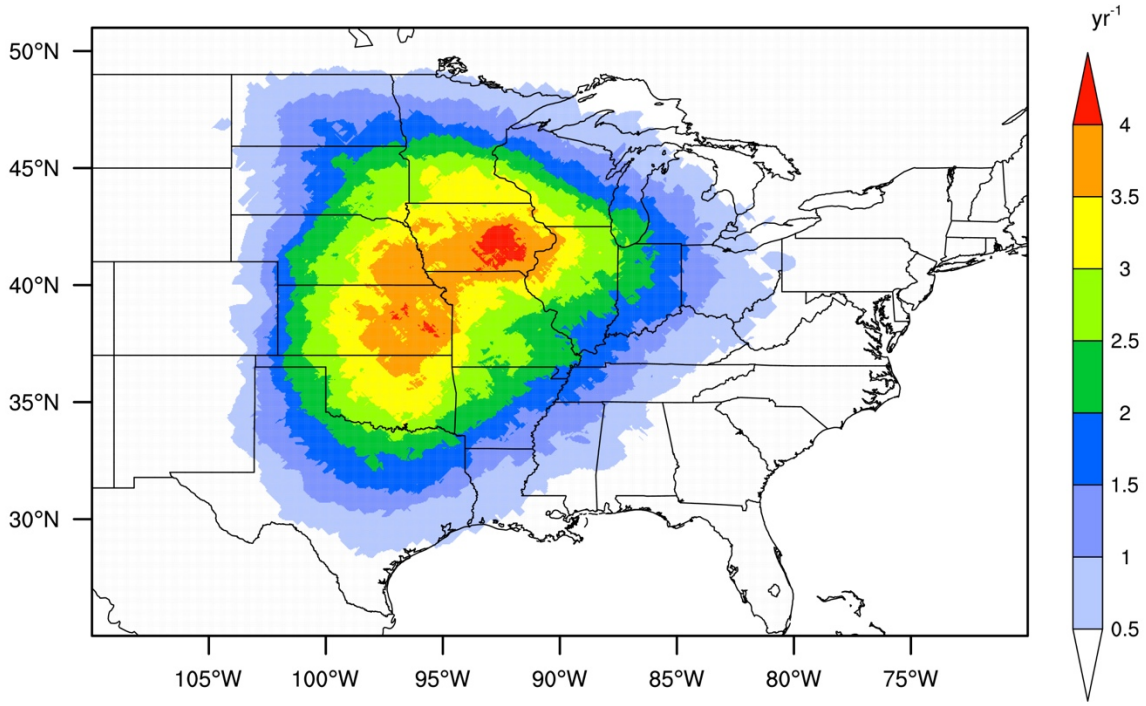

Figure 9. Spatial distribution of yearly averaged annual derecho numbers (ISD-based) over the United States east of the Rocky Mountains between 2004 and 2021. Here, we use derecho areas as derecho spatial coverages.

6.2 Monthly statistics

Figure 10 displays the yearly averaged seasonal variations in the derecho count, with remarkably more derechos in the warm than cold seasons, a feature consistent between ISD- and SED-based datasets and widely captured by previous studies (Ashley and Mote, 2005; Squitieri et al., 2023; Bentley and Sparks, 2003). However, our dataset has almost no derechos in the code season, which is generally not the case in previous studies. We attribute the difference to our usage of a physically-based derecho definition, which excludes many externally forced convective systems (e.g., extratropical cyclones), which are considered serial derechos in previous studies.

Figure 11 shows the spatial distributions of the monthly-mean derecho counts based on ISD between 2004 and 2021. On the one hand, many more derechos occur in the warm than cold months. On the other hand, we find remarkable shifts in the areas with the most frequent derecho occurrences from April to August. The region with the most derechos moves northward during the warm season. The northward

shifts resemble the MCS events (Li et al., 2021). We can identify two axes with frequent derecho occurrences. One is in the south-north direction along the Great Plains (e.g., June), and the other is in the west-east direction along the northern Great Plains and Midwest (e.g., July). The axes may represent the two types (serial and progressive) of derechos mentioned in Squitieri et al. (2023). A follow-up study will be conducted to investigate the large-scale environmental conditions associated with different types of derechos based on the developed derecho dataset. The SED-based dataset shows similar features but with much fewer derechos in June (Figure S7).

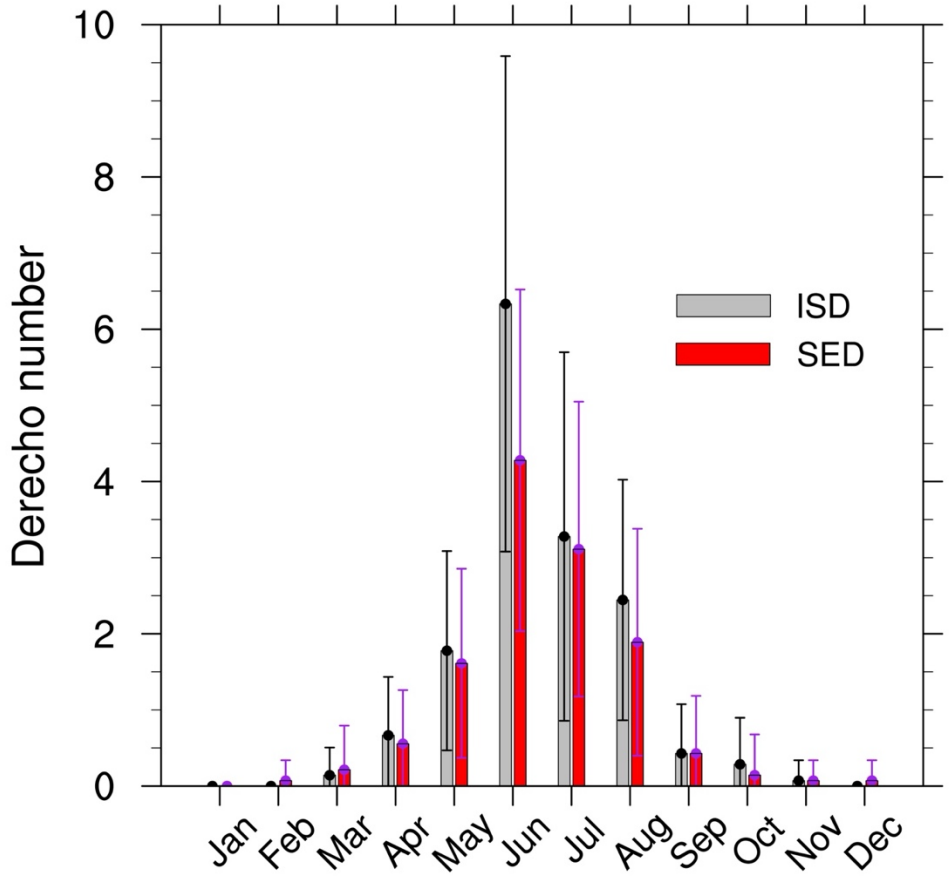

Figure 10. Yearly averaged monthly variations of the derecho numbers between 2004 and 2021. The error bars denote standard deviations. Gray is for ISD-based derechos, and red colors indicate SED-based derechos.

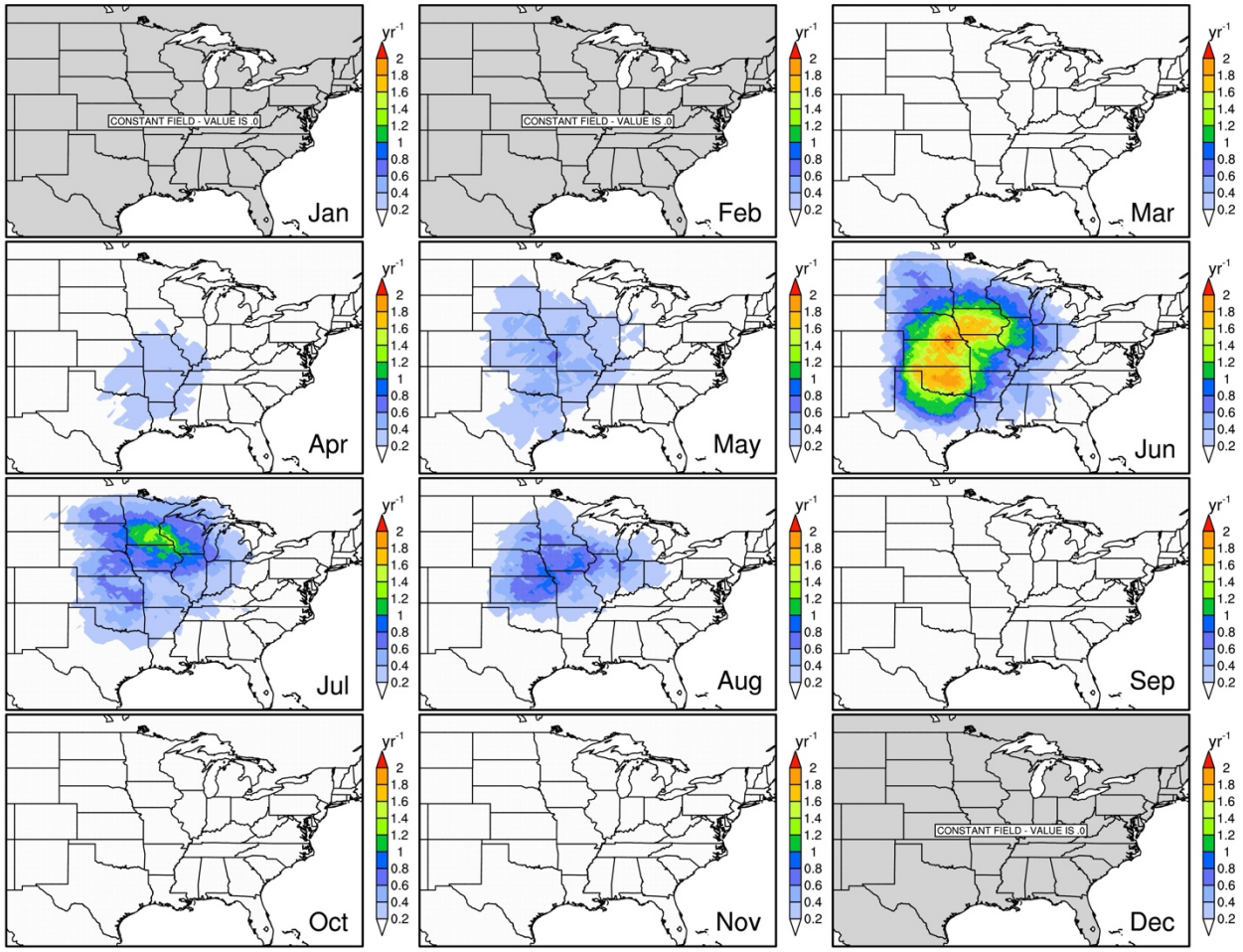

Figure 11. Same as Figure 9 but for yearly averaged monthly derecho numbers (ISD-based) over 2004-2021.

6.3 Wind damage characteristics

We examine the contributions of DMCSs and derechos to ISD damaging gust reports in the United States within our dataset from 2004 to 2021 (Figures 12, S2, and S8). Overall, MCSs contribute about 15.6% of all damaging gust reports, with the vast majority occurring east of the Rocky Mountains. On average, DMCSs contribute 4.0%, and derechos contribute 3.1% of all damaging gust occurrences. This indicates that about one quarter of the damaging gusts associated with MCS events are linked to DMCSs, much higher than the fraction (~3.5%) of DMCSs in MCSs. This finding aligns with the higher probabilities of extreme gusts in the gust speed PDF of DMCSs compared to general MCSs, indicating that DMCSs are more likely to produce extreme gusts than general MCSs (Figure S9). Understanding the

mechanisms behind their contrast will be a key focus of a follow-up study. Additionally, approximately 75% of DMCS-associated damaging gusts occur during the derecho period, reinforcing the validity of our derecho definition. As expected, the highest contributions of derechos to damaging gust reports are found in the Great Plains and Midwest (Figure 12).

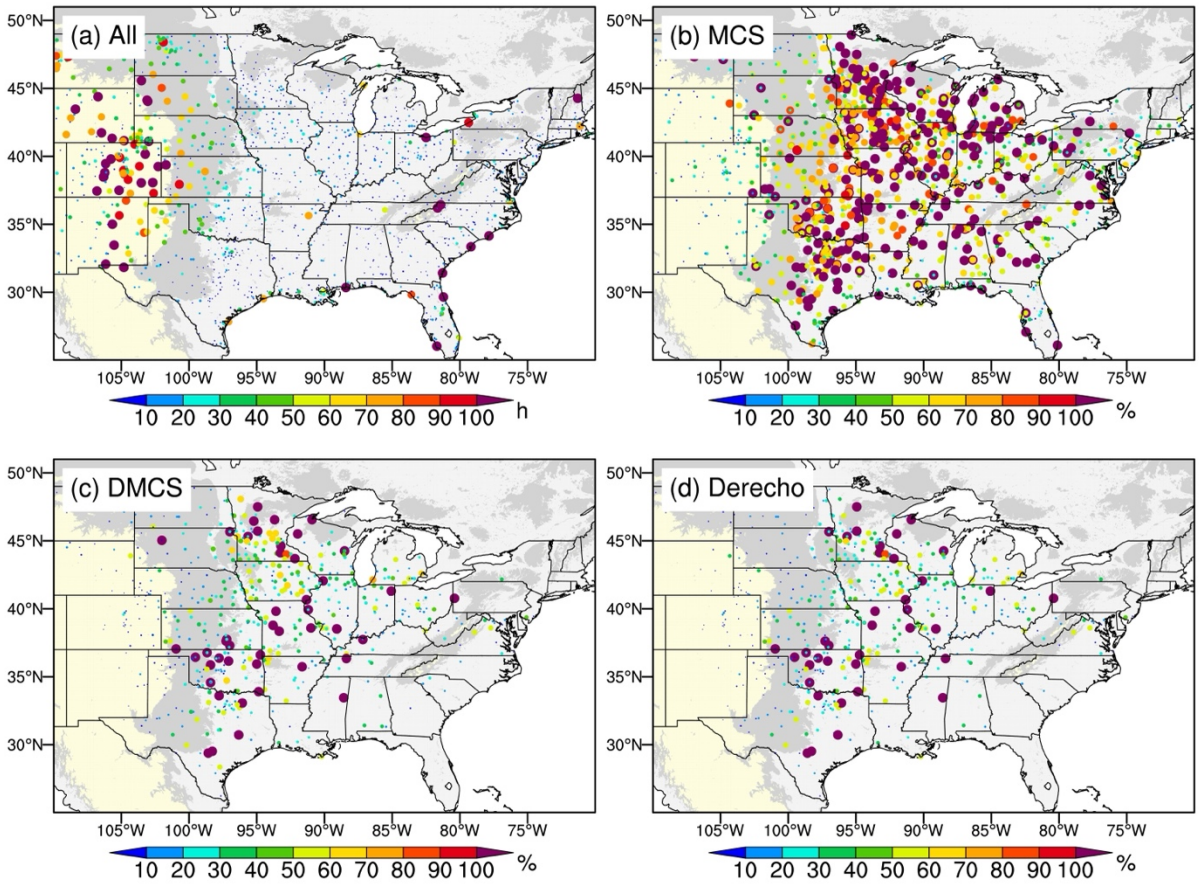

Figure 12. (a) The total numbers of damaging gust occurrences between 2004 and 2021 at ISD weather stations over the United States east of the Rocky Mountains. (b) Relative contributions of MCS events to the damaging gust occurrences in (a). (c) is the same as (b) but for relative contributions of DMCSs. (d) is the same as (c), but for derechos. Similar to Figure 5, we exclude non-derecho-producing MCS events overlapping with TCs in (b). The dot sizes are proportional to the corresponding values. Light-yellow shading denotes an elevation greater than 1000 m; light-gray shading denotes an elevation between 400 m and 1000 m; and smoke-white shading denotes an elevation less than 400 m. Background white is for oceans and lakes.

7 Data availability

The final ISD-based and SED-based derecho and DMCS dataset, along with the corresponding user guide, is publicly available at https://doi.org/10.5281/zenodo.14835362 (Li et al., 2025). The dataset is

stored in NetCDF-4 format and compressed by year for easier access. The user guide provides a detailed description of the data files, ensuring that users can effectively navigate and utilize the dataset.

For each pair of derecho and DMCS, the dataset includes two visualization figures (one for derecho and the one for the accompanying DMCS) illustrating the temporal evolutions of Z_{Hmax}, precipitation, wind speed, and gust speed throughout their respective lifetimes (e.g., Figures 13 and S10). These figures offer users an immediate understanding of the basic characteristics of each derecho and DMCS. The dataset also contains all the derecho-associated gust speeds and various parameter values used in the derecho definition. This allows users to further categorize derechos by intensity or type, following approaches similar to Coniglio and Stensrud (2004).

For researchers interested in applying the segmentation CNN for bow echo detection in different regions or time periods, or in leveraging the CNN-identified bow echoes for other studies, we provide access to the bow echo segmentation code and datasets at https://doi.org/10.5281/zenodo.10822721 (Geiss et al., 2024). This repository includes the trained CNN weights and detailed usage instructions. Additionally, a video supplement demonstrating the bow echo segmentation scheme is available at https://youtu.be/iHWY_OhaVUo and is permanently archived in the above Zenodo repository.

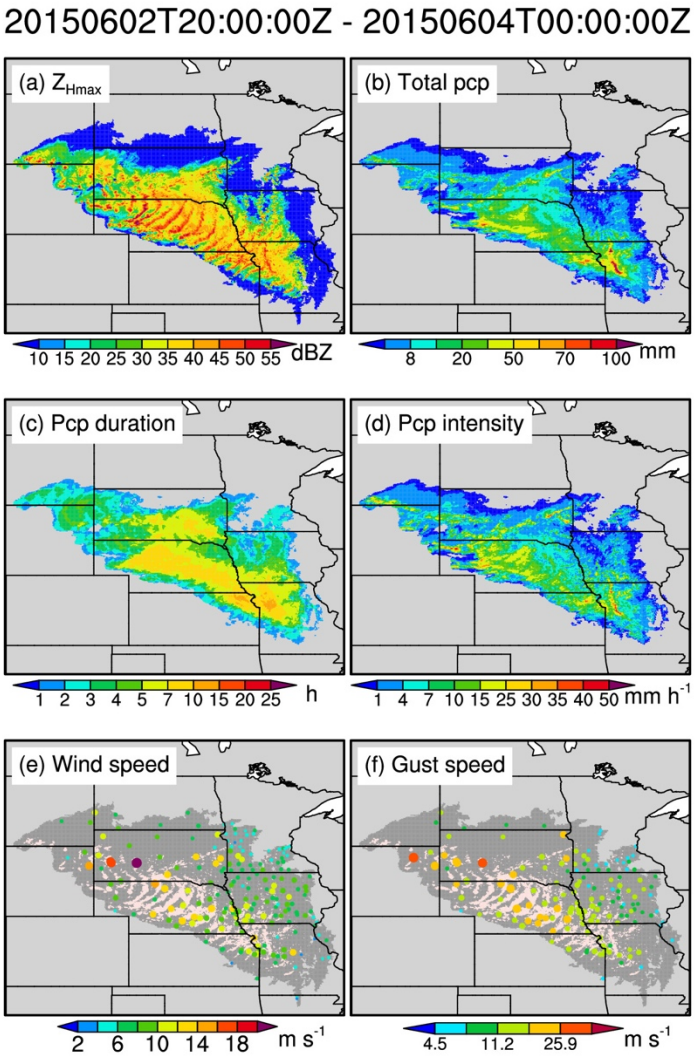

Figure 13. Similar to Figure 1 but for the spatial evolutions of (a) Z_{Hmax}, (b) total accumulated precipitation, (c) precipitation duration, (d) mean precipitation intensity, (e) hourly maximum wind speed, and (f) hourly maximum gust speed for a ISD-based DMCS that occurred on 2-4 June 2015. In (e) and (f), the misty rose shading corresponds to areas with $Z_{Hmax} \geq 40$ dBZ, and the dark gray shading refers to DMCS coverage with $Z_{Hmax} < 40$ dBZ. The figure title refers to the DMCS timing range.

8 Conclusions

This study presents a high-resolution (4 km and hourly) observational derecho dataset covering the United States east of the Rocky Mountains from 2004 to 2021. We develop the dataset using a combination of:

- An MCS dataset generated by the PyFLEXTRKR,

- Bow echoes identified by a semantic segmentation CNN,
- Hourly gust speed datasets from ISD or SED, and
- Physically based derecho identification criteria.

We evaluate the dataset and its potential uncertainties. The final dataset identifies 274 derechos using ISD gust measurements and 220 derechos using SED gust reports, with most events occurring in the warm season (April-August). Analyses indicate that derechos preferentially occur in the Great Plains and Midwest, with regions of highest frequency shifting northward from April to August. Derechos contribute 3.1% of ISD land-based damaging gusts over the United States between 2004 and 2021. Additionally, approximately 20% of MCS-associated damaging gusts are produced by derechos.

As the first derecho dataset that integrates machine-learning-based bow echo identification, physically based definition criteria, and two types of surface gust speed data, the dataset serves as an independent reference for derecho climatology, complementing previous studies. Beyond climatological analyses, the dataset can be used to:

- Investigate the derecho initiation and development mechanisms,
- Examine the environmental conditions that promote derecho formation and intensification,
- Assess the impacts of derechos on human safety and property, and
- Select specific events for case studies or to evaluate the numerical model simulations, thanks to its high spatiotemporal resolution.

Lastly, we emphasize that the automated derecho detection algorithm developed in this study is versatile and applicable to both observations and model results. The algorithm can be used to assess model performance and explore the impact of various factors on derechos (Kaminski et al., 2025).

Appendix A

For each bow echo in the derecho bow echo series, we use the formulas from the MATrix LABoratory (MATLAB) "regionprops" function (https://github.com/SBU-BMI/nscale/blob/master/original-matlab/features/regionprops.m; last access: January 28, 2025) to calculate its orientation. Then we apply the three-sigma rule to the orientations to remove outliers until all the rest orientations lie within three standard deviations of their mean. The mean is the average bow echo orientation. Implementing the three-sigma rule aims to minimize the adverse impact of the segmentation CNN identification uncertainties on calculating the averaged bow echo orientation.

The bow echo series' propagation direction and speed are calculated as follows. Firstly, we compute the moving direction and speed between any two consecutive bow echoes from the series. As exemplified in Figure A1, we assume that the bow echo at time t_1 would move to the location of bow echo t_1' at time t_2 if the bow echo shape remained unchanged. The location of bow echo t_1' is determined by its spatial correlation coefficient with bow echo t_2, and the location with the largest spatial correlation coefficient is what we want. Since bow echoes t_1 and t_1' have the same shape, it is straightforward to calculate the moving direction and speed between them, which are considered the moving direction and speed between bow echoes t_1 and t_2. Compared to using the centroid points of bow echoes t_1 and t_2, our approach can reduce the calculation bias when bow echoes t_1 and t_2 have distinct shapes and sizes. After we obtain all the moving directions and speeds between any two consecutive bow echoes, we apply the 1.5 × Interquartile Range (IQR) rule to remove outliers, considering potential CNN bow echo identification errors. Lastly, the median of the remaining moving speed values is considered the bow echo series' propagation speed, while the average of the remaining move direction values is considered the bow echo series' propagation direction.

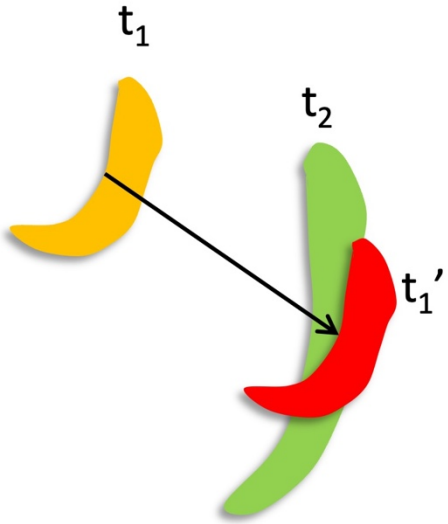

Figure A1. Schematic of the bow echo moving direction and speed calculation between two consecutive (t_1 and t_2) bow echoes. Bow echo t_1' is the same as bow echo t_1 but at a different location so that the spatial correlation coefficient between bow echoes t_1' and t_2 reaches the maximum. The moving direction and speed between bow echoes t_1 and t_1' are considered the moving direction and speed between bow echoes t_1 and t_2.

We use wind speeds at 500 hPa from ERA5 to compute the background mean wind speed. Considering the potential spatiotemporal variability of 500-hPa winds, we only count wind speeds covered by bow echoes from the bow echo series during the corresponding period. In detail, at time t_i during the bow echo series period (t_1–t_n), we only consider winds at time t_i but covered by bow echoes from time t_{i+1} to $min(t_{i+3}, t_n)$. Here, we exclude the bow echo at time t_i to minimize the potential impact of the bow echo on the background environment, while using up to three hours (t_{i+1}–t_{i+3}) of bow echoes aims to reduce the potential spatial noise since a bow echo is often too small. We average all wind speeds obtained from the above procedure to derive the background mean wind speed.

Author Contributions

JL, ZF, and LRL designed the study. JL prepared the input files for PyFLEXTRKR, and ZF ran PyFLEXTRKR to generate the MCS dataset. JL and ZF generated the initial positive and negative bow echo samples. AG trained and validated the CNN model. AG applied the trained semantic segmentation CNN to identify bow echoes from the MCS dataset with discussions with JL and ZF. JL defined and

identified derechos with discussions with ZF. JL evaluated the derecho dataset and manually examined the data. JL analyzed the derecho climatology with discussions with ZF. JL wrote the manuscript except for the machine-learning part which was written by AG. All co-authors reviewed the manuscript.

Competing Interests

The authors declare that they have no conflict of interest.

Acknowledgments

The NOAA SPC derechos and near-derechos are available at https://www.spc.noaa.gov/misc/AbtDerechos/annualevents.htm (last access: November 17, 2023). The named derechos we use to generate bow echo samples are from https://en.wikipedia.org/wiki/List_of_derecho_events (last access: 19 March 2023). The elevation data is from http://iridl.ldeo.columbia.edu/SOURCES/.NOAA/.NGDC/.GLOBE/ (last access: March 7, 2024). The IBTrACS Version 4 TC data over the North Atlantic basin is from https://doi.org/10.25921/82ty-9e16 (Knapp et al., 2018). Thank Drs. Israel L. Jirak, Brian J. Squitieri, and Andrew R. Wade from NOAA SPC for discussing the derecho definition criteria with us.

Financial support

This research is supported by the Regional and Global Model Analysis and Multisector Dynamics program areas of the U.S. Department of Energy Office of Science Biological and Environmental Research as part of the HyperFACETS project. PNNL is operated for the Department of Energy by Battelle Memorial Institute under Contract DE-AC05-76RL01830.

References

Adams-Selin, R. D. and Johnson, R. H.: Mesoscale surface pressure and temperature features associated with bow echoes, Monthly Weather Review, 138, 212-227, https://doi.org/10.1175/2009MWR2892.1, 2010.

Ardon-Dryer, K., Gill, T. E., and Tong, D. Q.: When a Dust Storm Is Not a Dust Storm: Reliability of Dust Records From the Storm Events Database and Implications for Geohealth Applications, GeoHealth, 7, e2022GH000699, https://doi.org/10.1029/2022GH000699, 2023.

Ashley, W. S. and Mote, T. L.: Derecho hazards in the United States, Bulletin of the American Meteorological Society, 86, 1577-1592, https://doi.org/10.1175/BAMS-86-11-1577, 2005.

Bardis, M., Houshyar, R., Chantaduly, C., Ushinsky, A., Glavis-Bloom, J., Shaver, M., Chow, D., Uchio, E., and Chang, P.: Deep learning with limited data: Organ segmentation performance by U-Net, Electronics, 9, 1199, https://doi.org/10.3390/electronics9081199, 2020.

Bentley, M. L. and Mote, T. L.: A climatology of derecho-producing mesoscale convective systems in the central and eastern United States, 1986–95. Part I: Temporal and spatial distribution, Bulletin of the American Meteorological Society, 79, 2527-2540, https://doi.org/10.1175/1520-0477(1998)079<2527:ACODPM>2.0.CO;2, 1998.

Bentley, M. L. and Sparks, J. A.: A 15 yr climatology of derecho-producing mesoscale convective systems over the central and eastern United States, Climate research, 24, 129-139, https://www.jstor.org/stable/24868368, 2003.

Bishop, C. M.: Pattern recognition and machine learning, Information Science and Statistics, 4, Springer, New York, NY, 2006.

Bowman, K. P. and Homeyer, C. R.: GridRad - Three-Dimensional Gridded NEXRAD WSR-88D Radar Data, the National Center for Atmospheric Research, Computational and Information Systems Laboratory [dataset], https://doi.org/10.5065/D6NK3CR7, 2017 (last access: 3 November 2022).

CDIACS/EOL/NCAR/UCAR and CPC/NCEP/NWS/NOAA: NCEP/CPC Four Kilometer Precipitation Set, Gauge and Radar, the National Center for Atmospheric Research, Computational and Information Systems Laboratory [dataset], https://doi.org/10.5065/D69Z93M3, 2000 (last access: 31 October 2022).

Coniglio, M. C. and Stensrud, D. J.: Interpreting the climatology of derechos, Weather and forecasting, 19, 595-605, https://doi.org/10.1175/1520-0434(2004)019<0595:ITCOD>2.0.CO;2, 2004.

Corfidi, S. F., Coniglio, M. C., Cohen, A. E., and Mead, C. M.: A proposed revision to the definition of "derecho", Bulletin of the American Meteorological Society, 97, 935-949, https://doi.org/10.1175/BAMS-D-14-00254.1, 2016.

Evans, J. S. and Doswell, C. A.: Examination of derecho environments using proximity soundings, Weather and Forecasting, 16, 329-342, https://doi.org/10.1175/1520-0434(2001)016<0329:EODEUP>2.0.CO;2, 2001.

Feng, Z.: Mesoscale convective system (MCS) database over United States (V3) [dataset], https://doi.org/10.5439/1571643, 2024 (last access: 25 Feburary 2025).

Feng, Z., Hardin, J., Barnes, H. C., Li, J., Leung, L. R., Varble, A., and Zhang, Z.: PyFLEXTRKR: a flexible feature tracking Python software for convective cloud analysis, Geoscientific Model Development, 16, 2753-2776, https://doi.org/10.5194/gmd-16-2753-2023, 2023.

Feng, Z., Houze, R. A., Leung, L. R., Song, F., Hardin, J. C., Wang, J., Gustafson, W. I., and Homeyer, C. R.: Spatiotemporal characteristics and large-scale environments of mesoscale convective systems east of the Rocky Mountains, Journal of Climate, 32, 7303-7328, https://doi.org/10.1175/JCLI-D-19-0137.1, 2019.

Feng, Z., Leung, L. R., Liu, N., Wang, J., Houze Jr, R. A., Li, J., Hardin, J. C., Chen, D., and Guo, J.: A global high-resolution mesoscale convective system database using satellite-derived cloud tops, surface precipitation, and tracking, Journal of Geophysical Research: Atmospheres, 126, e2020JD034202, https://doi.org/10.1029/2020JD034202, 2021.

Fujita, T. T.: Proposed characterization of tornadoes and hurricanes by area and intensity, https://ntrs.nasa.gov/api/citations/19720008829/downloads/19720008829.pdf, 1971.

Galea, D., Ma, H.-Y., Wu, W.-Y., and Kobayashi, D.: Deep Learning Image Segmentation for Atmospheric Rivers, Artificial Intelligence for the Earth Systems, 3, 230048, https://doi.org/10.1175/AIES-D-23-0048.1, 2024.

Geiss, A. and Hardin, J. C.: Radar super resolution using a deep convolutional neural network, Journal of Atmospheric and Oceanic Technology, 37, 2197-2207, https://doi.org/10.1175/JTECH-D-20-0074.1, 2020.

Geiss, A., Li, J., Feng, Z., and Leung, L. R.: Bow echo detection and segmentation, Zenodo [dataset], https://doi.org/10.5281/zenodo.10822721, 2024 (last access: 15 March 2024).

Guastini, C. T. and Bosart, L. F.: Analysis of a progressive derecho climatology and associated formation environments, Monthly Weather Review, 144, 1363-1382, https://doi.org/10.1175/MWR-D-15-0256.1, 2016.

Hersbach, H., Bell, B., Berrisford, P., Biavati, G., Horányi, A., Muñoz Sabater, J., Nicolas, J., Peubey, C., Radu, R., Rozum, I., Schepers, D., Simmons, A., Soci, C., Dee, D., and Thépaut, J.-N.: ERA5 hourly data on single levels from 1940 to present, Copernicus Climate Change Service (C3S) Climate Data Store (CDS) [dataset], https://doi.org/10.24381/cds.adbb2d47, 2023 (last access: 1 November 2022).

Huang, G., Liu, Z., Pleiss, G., Van Der Maaten, L., and Weinberger, K. Q.: Convolutional networks with dense connectivity, IEEE transactions on pattern analysis and machine intelligence, 44, 8704-8716, https://doi.org/10.1109/TPAMI.2019.2918284, 2019.

Huang, H., Lin, L., Tong, R., Hu, H., Zhang, Q., Iwamoto, Y., Han, X., Chen, Y.-W., and Wu, J.: Unet 3+: A full-scale connected unet for medical image segmentation, ICASSP 2020-2020 IEEE international conference on acoustics, speech and signal processing (ICASSP), 1055-1059, https://doi.org/10.1109/ICASSP40776.2020.9053405, 2020.

Janowiak, J., Joyce, B., and Xie, P.: NCEP/CPC L3 Half Hourly 4km Global (60S - 60N) Merged IR V1, Goddard Earth Sciences Data and Information Services Center (GES DISC) [dataset], https://doi.org/10.5067/P4HZB9N27EKU, 2017 (last access: 27 September 2022).

Johns, R. H. and Hirt, W. D.: Derechos: Widespread convectively induced windstorms, Weather and Forecasting, 2, 32-49, https://doi.org/10.1175/1520-0434(1987)002<0032:DWCIW>2.0.CO;2, 1987.

Kaminski, K., Ashley, W. S., Haberlie, A. M., and Gensini, V. A.: Future Derecho Potential in the United States, Journal of Climate, 38, 3-26, https://doi.org/10.1175/JCLI-D-23-0633.1, 2025.

Ketkar, N.: Introduction to keras, Deep learning with Python: a hands-on introduction, 97-111, https://doi.org/10.1007/978-1-4842-2766-4_7, 2017.

Kingma, D. P. and Ba, J.: Adam: A method for stochastic optimization, arXiv preprint arXiv:1412.6980, https://doi.org/10.48550/arXiv.1412.6980, 2014.

Knapp, K. R., Diamond, H. J., Kossin, J. P., Kruk, M. C., and Schreck, C. J. I.: International Best Track Archive for Climate Stewardship (IBTrACS) Project, Version 4, [North Atlantic], NOAA National Centers for Environmental Information [dataset], https://doi.org/10.25921/82ty-9e16, 2018 (last access: 5 March 2024).

Knapp, K. R., Kruk, M. C., Levinson, D. H., Diamond, H. J., and Neumann, C. J.: The international best track archive for climate stewardship (IBTrACS) unifying tropical cyclone data, Bulletin of the American Meteorological Society, 91, 363-376, https://doi.org/10.1175/2009BAMS2755.1, 2010.

Kumler-Bonfanti, C., Stewart, J., Hall, D., and Govett, M.: Tropical and extratropical cyclone detection using deep learning, Journal of Applied Meteorology and Climatology, 59, 1971-1985, https://doi.org/10.1175/JAMC-D-20-0117.1, 2020.

Lagerquist, R., Turner, D., Ebert-Uphoff, I., Stewart, J., and Hagerty, V.: Using deep learning to emulate and accelerate a radiative transfer model, Journal of Atmospheric and Oceanic Technology, 38, 1673-1696, https://doi.org/10.1175/JTECH-D-21-0007.1, 2021.

Li, J., Feng, Z., Qian, Y., and Leung, L. R.: A high-resolution unified observational data product of mesoscale convective systems and isolated deep convection in the United States for 2004–2017, Earth Syst. Sci. Data, 13, 827-856, https://doi.org/10.5194/essd-13-827-2021, 2021.

Li, J., Geiss, A., Feng, Z., and Leung, L. R.: A derecho climatology over the United States from 2004 to 2021, Zenodo [dataset], https://doi.org/10.5281/zenodo.14835362, 2025 (last access: 7 February 2025).

Mounier, A., Raynaud, L., Rottner, L., Plu, M., Arbogast, P., Kreitz, M., Mignan, L., and Touzé, B.: Detection of bow echoes in kilometer-scale forecasts using a convolutional neural network, Artificial Intelligence for the Earth Systems, 1, e210010, https://doi.org/10.1175/AIES-D-21-0010.1, 2022.

NOAA/NCEI: Global Hourly - Integrated Surface Database (ISD), the National Oceanic and Atmospheric Administration (NOAA) National Centers for Environmental Information (NCEI) [dataset], https://www.ncei.noaa.gov/data/global-hourly/archive/isd/, 2001 (last access: 21 January 2023).

NOAA/NCEI: Federal Climate Complex Data Documentation For Integrated Surface Data (ISD), 126, https://www.ncei.noaa.gov/data/global-hourly/doc/isd-format-document.pdf, 2018.

NOAA/NCEI: Storm Events Database [dataset], https://www.ncdc.noaa.gov/stormevents/, 2025 (last access: 27 August 2024).

Ouali, Y., Hudelot, C., and Tami, M.: An overview of deep semi-supervised learning, arXiv preprint arXiv:2006.05278, https://doi.org/10.48550/arXiv.2006.05278, 2020.

Peláez-Vegas, A., Mesejo, P., and Luengo, J.: A Survey on Semi-Supervised Semantic Segmentation, arXiv preprint arXiv:2302.09899, https://doi.org/10.48550/arXiv.2302.09899, 2023.

Ronneberger, O., Fischer, P., and Brox, T.: U-net: Convolutional networks for biomedical image segmentation, Medical Image Computing and Computer-Assisted Intervention–MICCAI 2015: 18th International Conference, Munich, Germany, October 5-9, 2015, Proceedings, Part III 18, 234-241, https://doi.org/10.1007/978-3-319-24574-4_28,

Santos, R. P. d.: Some comments on the reliability of NOAA's Storm Events Database, arXiv preprint, https://doi.org/10.48550/arXiv.1606.06973, 2016.

Sha, Y., Gagne II, D. J., West, G., and Stull, R.: Deep-learning-based gridded downscaling of surface meteorological variables in complex terrain. Part I: Daily maximum and minimum 2-m temperature, Journal of Applied Meteorology and Climatology, 59, 2057-2073, https://doi.org/10.1175/JAMC-D-20-0057.1, 2020.

Smith, A., Lott, N., and Vose, R.: The integrated surface database: Recent developments and partnerships, Bulletin of the American Meteorological Society, 92, 704-708, https://doi.org/10.1175/2011BAMS3015.1, 2011.

Squitieri, B. J., Wade, A. R., and Jirak, I. L.: A historical overview on the science of derechos: part I: identification, climatology, and societal impacts, Bulletin of the American Meteorological Society, 104, E1709-E1733, https://doi.org/10.1175/BAMS-D-22-0217.1, 2023.

Starzec, M., Homeyer, C. R., and Mullendore, G. L.: Storm labeling in three dimensions (SL3D): A volumetric radar echo and dual-polarization updraft classification algorithm, Monthly Weather Review, 145, 1127-1145, https://doi.org/10.1175/MWR-D-16-0089.1, 2017.

Taha, A. A. and Hanbury, A.: Metrics for evaluating 3D medical image segmentation: analysis, selection, and tool, BMC medical imaging, 15, 1-28, https://doi.org/10.1186/s12880-015-0068-x, 2015.

Van Engelen, J. E. and Hoos, H. H.: A survey on semi-supervised learning, Machine learning, 109, 373-440, https://doi.org/10.1007/s10994-019-05855-6, 2020.

Weisman, M. L.: The genesis of severe, long-lived bow echoes, Journal of the Atmospheric Sciences, 50, 645-670, https://doi.org/10.1175/1520-0469(1993)050<0645:TGOSLL>2.0.CO;2, 1993.

Weyn, J. A., Durran, D. R., Caruana, R., and Cresswell-Clay, N.: Sub-seasonal forecasting with a large ensemble of deep-learning weather prediction models, Journal of Advances in Modeling Earth Systems, 13, e2021MS002502, https://doi.org/10.1029/2021MS002502, 2021.

White, C. H., Ebert-Uphoff, I., Haynes, J. M., and Noh, Y.-J.: Super-Resolution of GOES-16 ABI Bands to a Common High Resolution with a Convolutional Neural Network, Artificial Intelligence for the Earth Systems, https://doi.org/10.1175/AIES-D-23-0065.1, 2024.

Whitehall, K., Mattmann, C. A., Jenkins, G., Rwebangira, M., Demoz, B., Waliser, D., Kim, J., Goodale, C., Hart, A., and Ramirez, P.: Exploring a graph theory based algorithm for automated identification and characterization of large mesoscale convective systems in satellite datasets, Earth Science Informatics, 8, 663-675, https://doi.org/10.1007/s12145-014-0181-3, 2015.